AD

AD-E403 933

Technical Report ARMET-TR-16076

155-MM M795 AEROFUZE TEST AT THE KOFA RANGE, YUMA PROVING GROUND, ARIZONA, 19 MAY 2015

Aaron Barton

September 2017

U.S. ARMY ARMAMENT RESEARCH, DEVELOPMENT AND ENGINEERING CENTER

Munitions Engineering Technology Center

Picatinny Arsenal, New Jersey

REPORT DOCUMENTATION PAGE

Form Approved
OMB No. 0704-01-0188

1. REPORT DATE (DD-MM-YYYY)	2. REPORT TYPE	3. DATES COVERED (*From - To*)
September 2017	Final	May 2015 to June 2015

4. TITLE AND SUBTITLE

155-MM M795 AEROFUZE TEST AT THE KOFA RANGE, YUMA PROVING GROUND, ARIZONA, 19 MAY 2015

5a. CONTRACT NUMBER

5b. GRANT NUMBER

5c. PROGRAM ELEMENT NUMBER

6. AUTHORS

Aaron Barton

5d. PROJECT NUMBER

5e. TASK NUMBER

5f. WORK UNIT NUMBER

7. PERFORMING ORGANIZATION NAME(S) AND ADDRESS(ES)

U.S. Army ARDEC, METC
Fuze & Precision Armaments Directorate
(RDAR-MEF-I)
Picatinny Arsenal, NJ 07806-5000

8. PERFORMING ORGANIZATION REPORT NUMBER

9. SPONSORING/MONITORING AGENCY NAME(S) AND ADDRESS(ES)

U.S. Army ARDEC, ESIC
Knowledge & Process Management (RDAR-EIK)
Picatinny Arsenal, NJ 07806-5000

10. SPONSOR/MONITOR'S ACRONYM(S)

11. SPONSOR/MONITOR'S REPORT NUMBER(S)

Technical Report ARMET-TR-16076

12. DISTRIBUTION/AVAILABILITY STATEMENT

Approved for public release; distribution is unlimited.

13. SUPPLEMENTARY NOTES

14. ABSTRACT

The Aerofuze system is a projectile diagnostic telemeter for mortars and artillery. Developed to collect in-bore and in-flight dynamics including spin, pitch, yaw, and 3-axis acceleration in real time, data is relayed to a ground station using an integrated S-band transmitter. One unit was successfully fired on a M795 spotter projectile at Yuma Proving Ground, AZ, in May 2015. The unit was fired twice prior in the 155-mm Air Gun at the U.S Army Armament, Research and Development Center, Picatinny Arsenal, NJ. The system telemetered 51 sec of uninterrupted aeroballistics data, capturing both in-bore and in-flight data, which is presented in this report.

15. SUBJECT TERMS

Telemetry High acceleration High-g Gun launched DFuze Aerofuze

16. SECURITY CLASSIFICATION OF:			17. LIMITATION OF ABSTRACT	18. NUMBER OF PAGES	19a. NAME OF RESPONSIBLE PERSON
a. REPORT	b. ABSTRACT	c. THIS PAGE			Aaron E. Barton
U	U	U	SAR	49	19b. TELEPHONE NUMBER (Include area code) (973) 724-3521

Standard Form 298 (Rev. 8/98)
Prescribed by ANSI Std. Z39.18

CONTENTS

FIGURES

FIGURES
(continued)

FIGURES
(continued)

ACKNOWLEDGMENTS

The author wishes to express his sincere gratitude to the following people for supporting this effort: Patrick Sweeney and Richard Granitzki for their telemetry support; Mike Hollis, Eric Marshall, Joel Metz, Gary Dundon, and Frank Munoz for their role in mechanical design and stress analysis; Andy Del Valle and Dave Pritchard for their role in assembling the test articles; Mike Menegus for his air gun testing support; Jim Granitzki and Bill Bakula for their machining support; Richard Siegal and Chris Harkins for their transmitter support; and Dr. Myron Hohil, Craig Sandberg, Bill Osborne, and Sal Longo for their support in obtaining necessary program funds. Finally, he wishes to thank his family for their love and support.

INTRODUCTION

The Aerofuze program successfully tested one unit on a M795 spotter projectile at Yuma Proving Ground (YPG), AZ. The unit was fired twice prior in the 155-mm Air Gun at the U.S. Army Armament, Research and Development (ARDEC), Picatinny Arsenal, NJ. The two main objectives for the test were: (1) to determine functionality of the Aerofuze system under live fire, and (2) if the system is functional, observe data to learn typical performance characteristics. No issues with overall system health were observed during gun launch and flight. The system telemetered 51 sec of uninterrupted aeroballistics data, capturing both interior and exterior ballistic information, which is presented in this report.

AEROFUZE BACKGROUND

The Aerofuze system is a projectile aeroballistics diagnostic telemeter for mortars and artillery. Developed to collect in-flight dynamics including spin, pitch, yaw, and 3-axis acceleration in real time, data is relayed to a ground station using an integrated S-band transmitter. Packaged as either a mortar standard fuze or a North Atlantic Treaty Organization (NATO) standard fuze, Aerofuze can be used on all 60/81/120-mm mortars or 105/155 artillery shells. For all other rounds, a modular design allows the Aerofuze hardware to be integrated in any 40-mm or larger cylindrical form factor. Figure 1 is a computer-aided design (CAD) rendering of the NATO Aerofuze showing a cross-sectional view as well as the isometric view with the printed circuit board (PCB) visible.

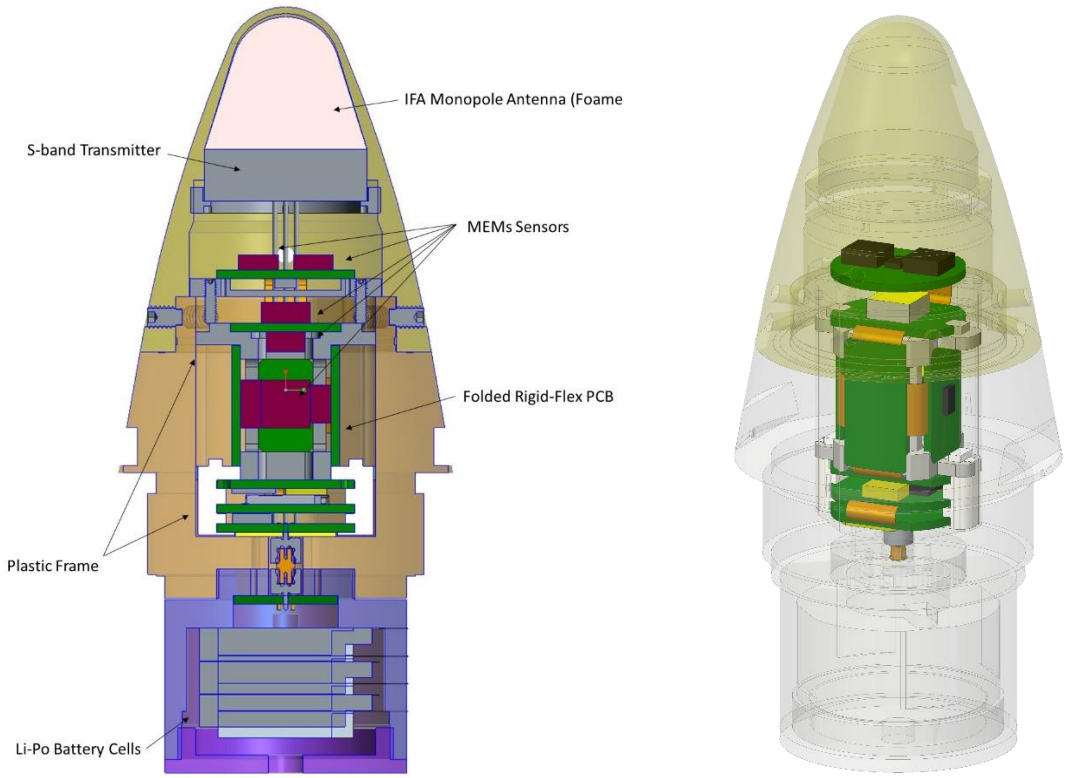

(a)
Cross section

(b)
Isometric with PCB visible

Figure 1
CAD renderings of the Aerofuze in the NATO fuze housing

The system consists of a series of micro-electromechanical systems (MEMS) accelerometer and gyroscope sensors, signal conditioning circuitry, analog-to-digital converter circuitry, a low-power, field-programmable gate array (FPGA) processor, and a Microwave Innovations, Furlong, PA, miniature S-band pulse code modulation/frequency modulation (PCM/FM) transmitter. There is also 2 Mbit of static random-access memory available to buffer data. On each of the system's principle axes (as diagramed in figure 2), there is a high-g accelerometer, a low-g accelerometer, a high-rate MEMS gyroscopes, and a low-rate MEMS gyroscopes. There are also two, 3-axis magnetometers located within the nosecone. Circuitry is included to optionally support four U.S. Army Research Laboratory, Aberdeen Proving Ground, MD, Solar Likeness Indicating Transducer (SLIT) solar sensors (ref. 1). The system is powered by four 3.7-V lithium polymer battery cells.

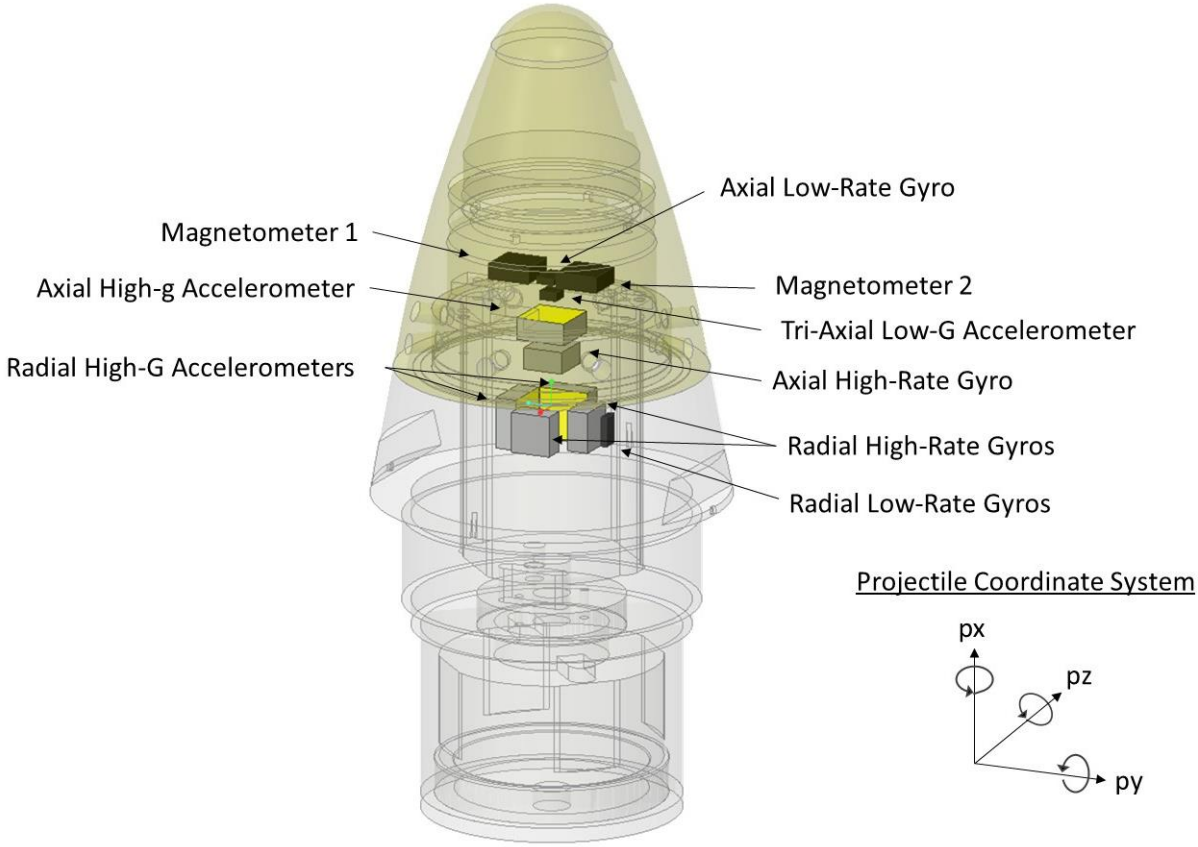

Figure 2
Diagram of the Aerofuze projectile coordinate system with MEMS sensors annotated

The system was designed using rigid-flex PCB technology for ease of assembly (fig. 3). The sensors are mounted on a board that folds into a cube shape, which is then fitted over a three-dimensional selective laser sintered printed plastic frame. The assembly is then dropped into its associated metal housing, which is in the outer shape of a projectile fuze. The S-band transmitter is integrated into the nosecone of the body and uses a custom inverted-F antenna (IFA) developed by the author as is pictured in figure 4. This antenna is foamed into the nosecone cavity using ECCOSTOCK material for survivability and, combined with the projectile body, provides a dipole-like radiation pattern, providing full azimuthal coverage around the center axis.

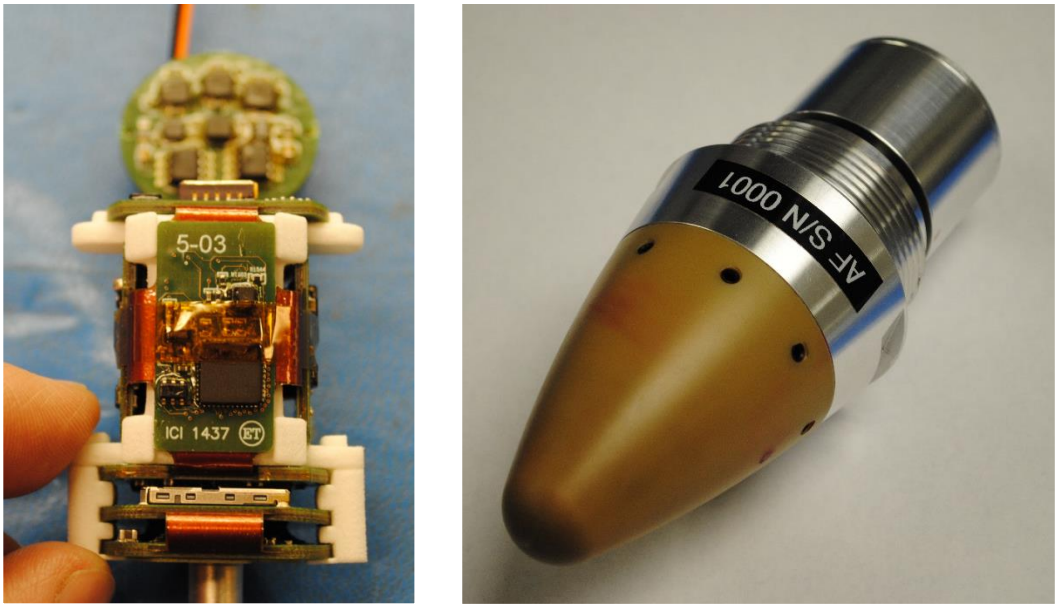

(a)
Rigid-flex PCB board stack

(b)
Full assembled NATO fuze housing

Figure 3
Aerofuze, unit serial no. (SN) 0001

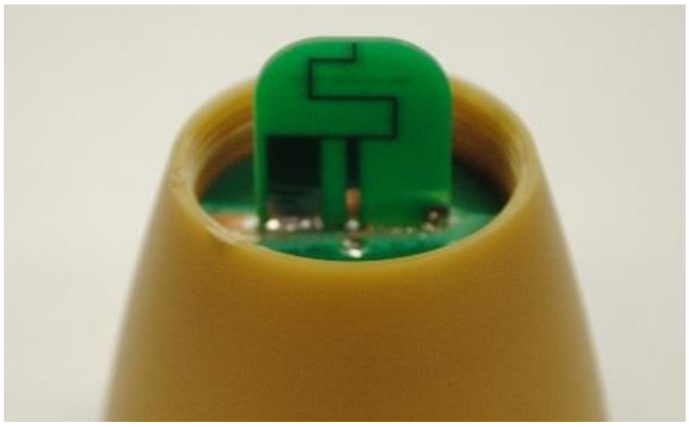

Figure 4
Nosecone IFA for S-band telemetry

PRIOR TESTING

The Aerofuze SN0001 unit was fired in the 155-mm Air Gun at ARDEC on April 2, 2015 and again on April 3, 2015. The first test firing was set for a target of 20,000-g acceleration with spin. The device was programmed to trigger on spin and delay-repeat 200 ms of data. However, the unit accidentally triggered earlier than setback; it is speculated that it triggered while loading into the gun. The unit survived the test firing and was still functional. The unit was tested a second time on the next day, again in the 155-mm Air Gun, with a target of 8,500-g acceleration with spin. The unit was reprogrammed to trigger at a higher spin level and was programmed to ignore all trigger signals

within the first 5 min after turned on, serving as an arming delay. The unit survived the test firing, and data was collected.

At the end of April 2015, there was an opportunity to live-fire the unit by piggybacking on the Chrome M777 1B-Blowby (1BB) test. The test required S-band telemetry, along with two M795 spotters, which the Aerofuze unit could be mounted onto one of them. New batteries for the unit were built, potted, and charged. The unit was laboratory tested and shipped with batteries and supporting hardware.

LIVE-FIRE TEST

On Monday, May 18, 2015, at gun location GP19-1 at YPG, a John Douglas Associates Decommutator/Breakout Box (JDA DECOM/BOB) was set up in the supporting telemetry van. Telemetry support included a tracking antenna and a fixed dual-polarization horn antenna. A check was conducted with the Aerofuze unit held in hand. Telemetry equipment was set up as depicted in figure 5. The radar tracking information was captured during the flight of the round as well as the muzzle exit velocity.

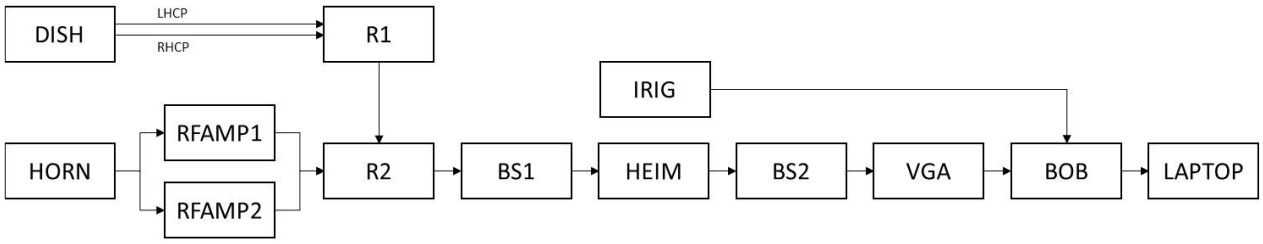

Figure 5
Block diagram of telemetry equipment setup

The unit was fired the next day on Tuesday May 19, 2015. Figure 6 shows the unit prior to live fire. The unit was activated by tightly screwing the battery pack and main assembly together. A DECOM lock was established and relayed to the gun crew before the round was screwed onto the projectile, which was the second M795 spotter round during the 1BB test. The round was fired approximately 3:09 min later, and the signal lock was retained throughout 51 sec of flight until impact. Table 1 is a list of the telemetry equipment. Figure 7 shows a photograph of the testing setup including the M777 artillery canon (middle), Telecommunication Systems (TCS) tracking antenna rotated backwards (left), and fixed horn antenna (right). Figure 8 shows a photograph of a fixed horn antenna (center) and TCS tracking antenna (right). Figure 9 shows a photograph of M777 artillery canon used in testing (center), and the fixed horn antenna is also shown (left-center).

Note: Photograph taken May 19, 2015.

Figure 6
Aerofuze SN0001 unit mounted to a M795 spotter projectile, immediately prior to live fire

Table 1
List of telemetry equipment

Name	Description
DISH	Tracking antenna
HORN	Dual-mode horn antenna
RFAMP1	Radio frequency (RF) amplifier
RFAMP2	RF amplifier
R1	Receiver
R2	Receiver
BS1	Bit sync
HEIM	Data recorder
BS2	Bit sync
VGA	Variable gain amplifer
BOB	Telemetry system
Inter-Range Instrumentation Group (IRIG)	IRIG timecode generator
LAPTOP	Telemetry decommutator (DECOM)

Note: Photograph taken May 19, 2015.

Figure 7
Photograph of testing setup

Note: Photograph taken May 19, 2015.

Figure 8
Photograph of fixed horn antenna (center) and TCS tracking antenna (right)

Figure 9
Photograph of M777 artillery canon used in testing (center) and fixed horn antenna (left-center)

DATA INFORMATION

Data was recorded at KOFA GP-19-1. Data was partially reduced at the gun location and later fully reduced at ARDEC. Tables 2 and 3 show this data.

Table 2
Summary of data information

Date	05/19/2015 (Tuesday)
Aerofuze S/N	0001
Data stream	10Mbit/sec NRZ-L
Sampling rate	14,204.54 samples/sec
Tube round no.	3050
Line of fire	97 deg
Quadrant elevation	444 mils (24.975 deg)
Fire time	139:17:44:03.967767
Projectile	M795 inert spotter
Gun	Chrome M777 – SN 002C
Gun tube length	198 in. (5.03 m)
Gun tube rifling twist rate	1/20 rev/caliber
Propellant charge	Modular artillery charge system-5-PIP

Table 3
Sensor data channels and filtering information

Data	No. of Channels	Components	Analog filtering
High-g accelerometers	3	(3X) Silicon designs SD1221L-20K	1-kHz 2-pole Butterworth Sallen-Key filter per channel
Low-g accelerometers	3	(1X) Analog devices ADXL377	500-Hz resistor-capacitor (RC) filter, followed by a 1 kHz Butterworth 2-pole Sallen-Key filter per channel
High-rate gyroscopes	3	(3X) Analog devices ADXRS649	1-kHz internal filter + 1kHz single-pole RC filter per channel
Low-rate gyroscopes	3	(3X) ST Microelectronics LY3100ALH	Internal RC filter (140 Hz). Additional filtering due to high output impedance and analog multiplexer capacitance (unknown cut-off frequency).
Magnetometer	6	(2X) Honeywell HMC1053	1-kHz 2-pole Butterworth Sallen-Key filter per channel
Battery voltage	1		2.3-kHz RC filter
Temperature	1	(1X) Texas Instruments LM94021	No filter
Runtime counter	1		
Ground channel	1		

CALIBRATION FACTORS

For this data reduction, bias levels (i.e., the analog-to-digital converter count value that is treated as the zero level) for the following are taken from samples prior to setback: high-g accelerometers, low-g accelerometer, high-g gyroscopes, and low-g gyroscopes. A zero level for temperature sensor is taken from the Texas Instruments LM94021 datasheet. Bias levels for the magnetometers are taken with the Aerofuze round and placed in a 3-axis Helmholtz coil, cancelling out the geomagnetic field.

For this data reduction, slope values for each sensor channel are derived from the nominal sensitivities of each sensor as given in their respective component datasheets (units/volt), then are converted from counts to volts (3V/4095), multiplied by gain and attenuation factors in the channel signal conditioning circuitry, and converted to final units. Table 4 shows the sensor sensitivities and bias levels.

Table 4
Sensor sensitivities and bias levels

Projectile axis name	Schematic name	Channel no.	Slope (unit/count)	Zero level (counts)	Units
batt_mon	batt_mon	9	3/4095/0.3546	0	V
temp	temp	30	-1*3/4095/.0109	2866	°C
gnd	gnd	49	3/4095	0	V
mag1_py	mag1_x	26	-1/(0.001*5*199.4*4095/3)	862	gauss
mag1_pz	mag1_y	12	1/(0.001*5*199.4*4095/3)	4095†	gauss
mag1_px	mag1_z	27	-1/(0.001*5*199.4*4095/3)	2189	gauss
mag2_pz	mag2_x	29	-1/(0.001*5*199.4*4095/3)	2013	gauss
mag2_py	mag2_y	47	-1/(0.001*5*199.4*4095/3)	2229	gauss
mag2_px	mag2_z	28	-1/(0.001*5*199.4*4095/3)	1926	gauss
la_py	la_x	14	-1*3/4095/0.007	2045	g
la_pz	la_y	13	3/4095/0.007	2045	g
la_px	la_z	15	-1*3/4095/0.007	2041	g
ha_px	ha_x	16	-1*3/4095/0.0002/0.595	2375	g
ha_pz	ha_y	18	-1*-1*3/4095/0.0002/0.595	2183	g
ha_py	ha_z	17	-1*3/4095/0.0002/0.595	2087	g
hgyro_px	gyro_x	48	(3/0.606)/4095/0.0001/360	2055	Hz
hgyro_pz	gyro_y	31	-1*(3/0.606)/4095/0.0001/360	2055	Hz
hgyro_py	gyro_z	39	(3/0.606)/4095/0.0001/360,	2053	Hz
lgyro_px	lgyro_x	25	1/(0.0011*360*4095/3)	2044	Hz
lgyro_pz	lgyro_y	46	1/(0.0011*360*4095/3)	2033	Hz
lgyro_py	lgyro_z	38	1/(0.0011*360*4095/3)	2033	Hz

† This channel was not responsive during calibration.

Each sensor originally had its own name within the electrical schematic of the Aerofuze system. For this data reduction, they have been renamed and aligned to match the projectile coordinate system (px,py,pz), as shown earlier in figure 2. The axis px is aligned with the projectile centerline and points out of the projectile nose, py points in the direction from magnetometer 1 to magnetometer 2, and pz is the orthogonal axis between px and py, creating a right-handed coordinate system. All rotations of the projectile also coincide to these axes, following the right-hand rule around each axis as the direction of positive rotation.

The 3-axis Helmholtz coil used to obtain calibration information for the magnetometers is pictured in figure 10. The Aerofuze unit was placed in the center of the coil using a plastic fixture that aligns the fuze body with the principle axis. Note that this did not include the M795 projectile body. The instrument acts to nullify the geomagnetic field by default. The values of the magnetometers at this time were treated as the channels' zero-bias levels. Magnetometer sensitives and cross-axis sensitivities were also collected but were not used in this data reduction.

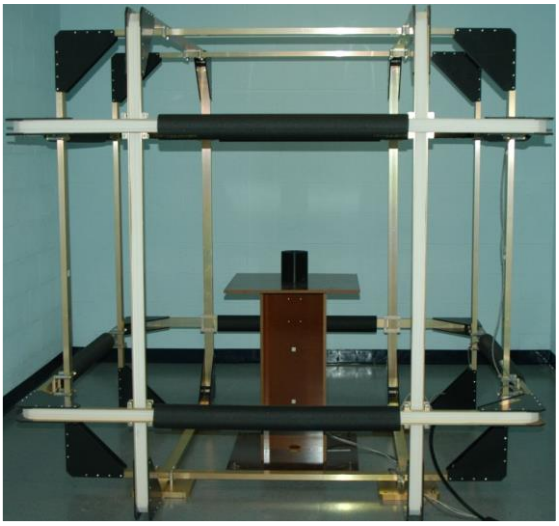

Figure 10
Photograph of 3-axis Helmholtz coil at ARDEC

RESULTS OF LIVE-FIRE TEST

Overall System Heath

No issues with overall system health were observed during gun launch and flight. There was 51 sec of uninterrupted telemetry data recorded after gun launch out of a total of 66.1 sec of total telemetry data recorded. A total of 15.1 sec of data is available as the round was idle in the gun tube. In-bore data was captured without issue due to the 200-ms live delay. No system resets were observed. No frame dropouts were observed within the 51-sec window after firing. Dropouts were observed toward the end of flight just before impact, which is normal. Battery voltage remained above 7.1V during both in-bore and in-flight events. Muzzle exit velocity was measured as 843.3 m/s using a Weibel SL-525PE Doppler radar system.

In-bore Data

High-g Accelerometers (3X SD1221L-20K)

Data was measured from three high-g accelerometers during in-bore acceleration (fig. 11). The axial high-g accelerometer data shows an acceleration curve consistent with gun launch. Peak acceleration was measured as 14,240 g. A large 12,160-g spike was seen as the projectile exited the tube. Radial high-g acceleration data also shows large spikes (5,627 g and 3,934 g) during tube-exit events with centrifugal force due to spin superimposed.

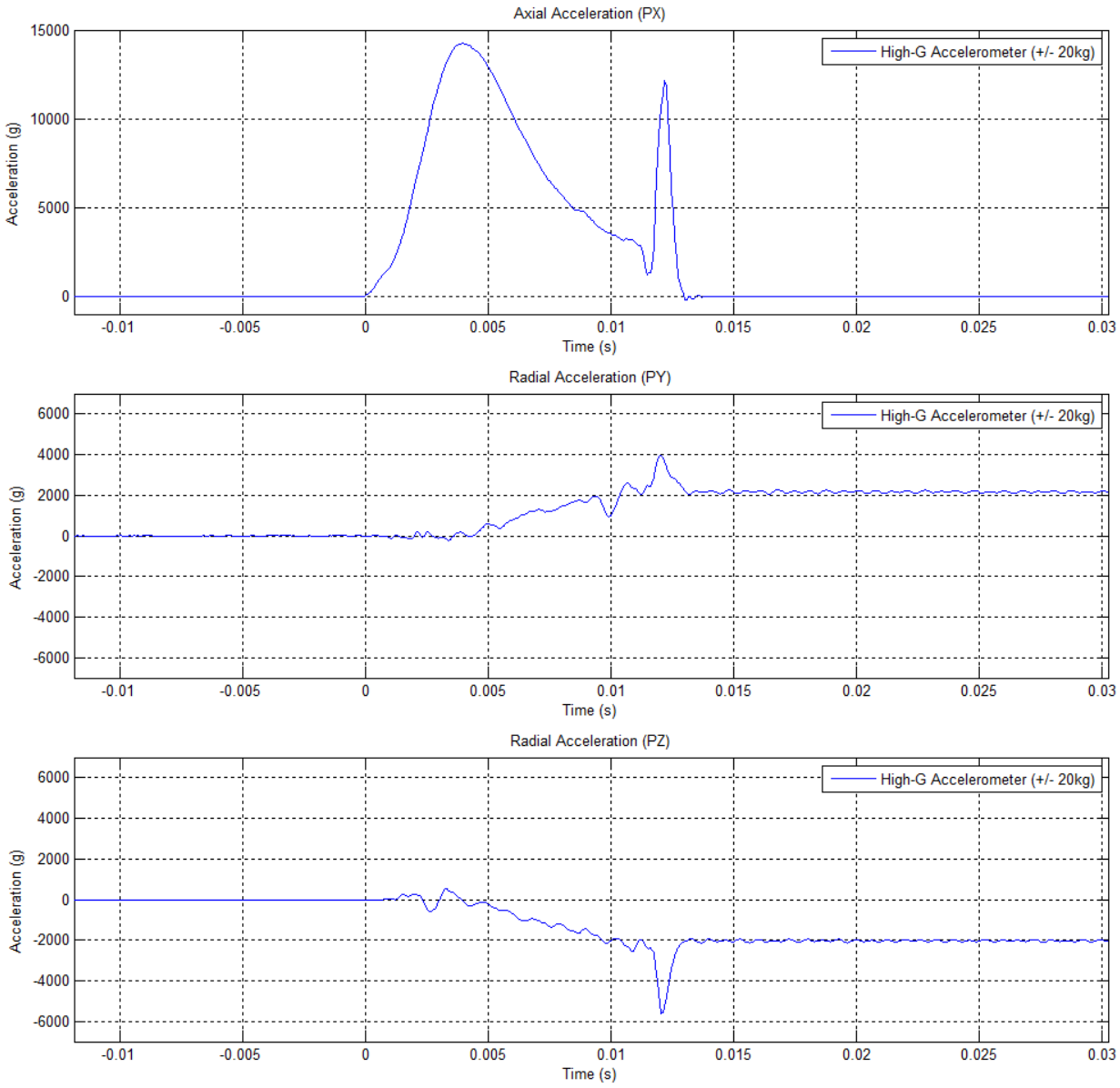

Figure 11
Plot of high-g accelerometer data during in-bore acceleration

Low-g Accelerometer (ADXL377)

Data was observed from the 3-axis, low-g accelerometer during the gun-launch event (fig. 12). During setback and set forward, the measured acceleration on each axis is mostly oscillating with the channels saturating. Oscillations can be observed after tube exit.

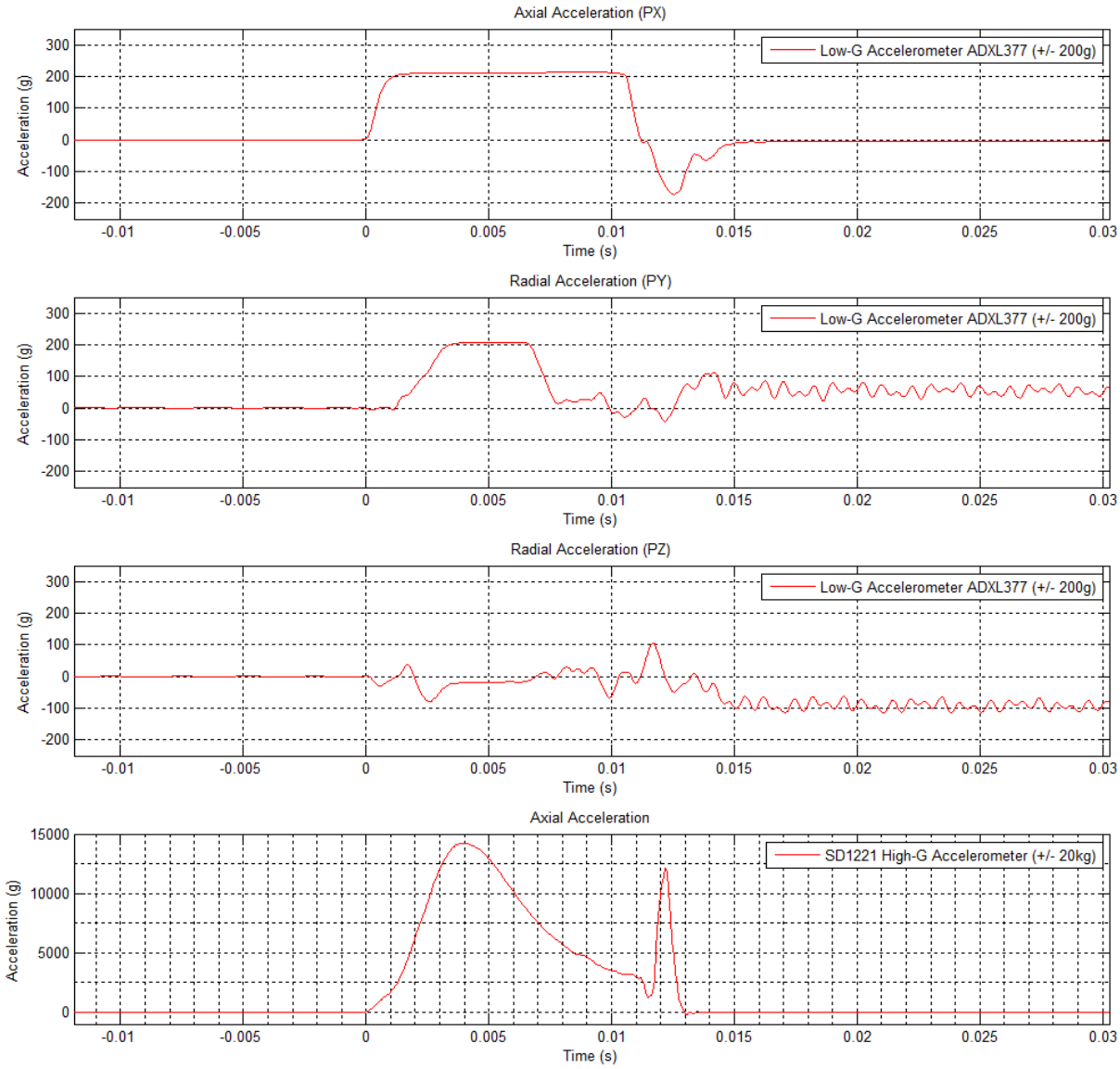

Note: High-g axial acceleration is shown to highlight setback and set forward events.

Figure 12
Plot of low-g accelerometer data during in-bore acceleration

The axial low-g accelerometer does capture the setback and set forward events, even though it saturates at 210 g and does not capture the high-frequency information that the high-g accelerometer captures. Figure 13 shows a plot of the axial high-g and low-g accelerometer data.

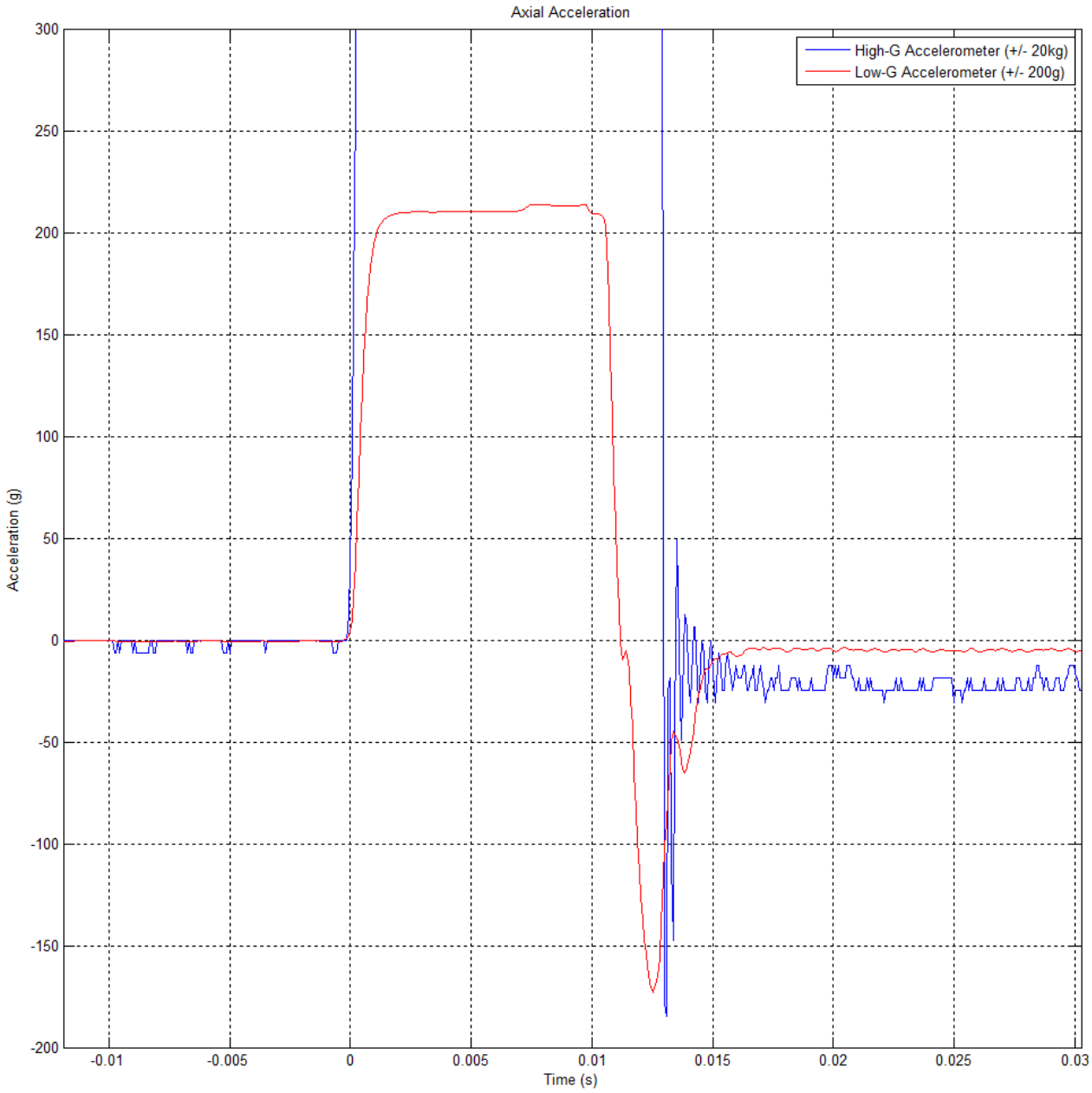

Figure 13
Superimposed plot of axial high-g and axial low-g accelerometer data during in-bore event

Magnetometer Data (2X HMC1053)

Magnetometer data during gun launch was collected as well. As the round exists the tube, the magnetometer data shows an expected sinusoidal wave on the radial axes. As expected, Mag_1_Y data is unavailable, as this channel was noted to be nonfunctional during assembly prior to air gun testing. Figure 14 shows the plot of calibrated magnetometer data during and just after tube exit. The high-g axial acceleration is shown to highlight setback and set forward times.

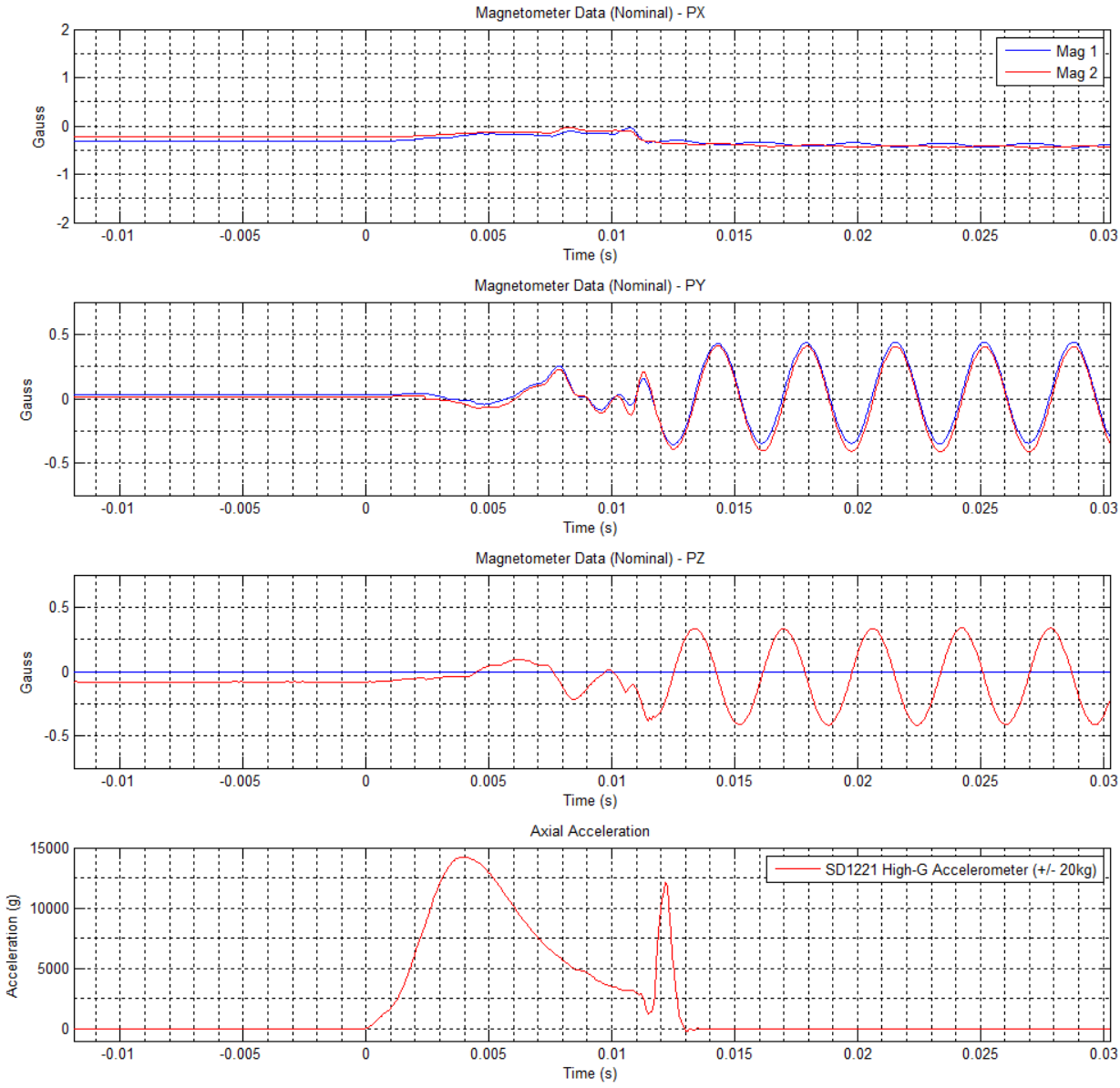

Figure 14
Plot of calibrated magnetometer data during and just after tube exit

Battery Voltage and Temperature

Battery voltage was measured during gun launch and showed oscillations during both setback and set forward events, remaining within 7.169 to 7.305V, which is well within operating limits. Temperature of the projectile remained mainly at 25°C while in bore. Some ringing in the temperature measurements was observed during setback and set forward. Figure 15 shows a plot of the battery voltage and temperature measurement during the in-bore event. High-g axial acceleration is shown to highlight setback and set forward times.

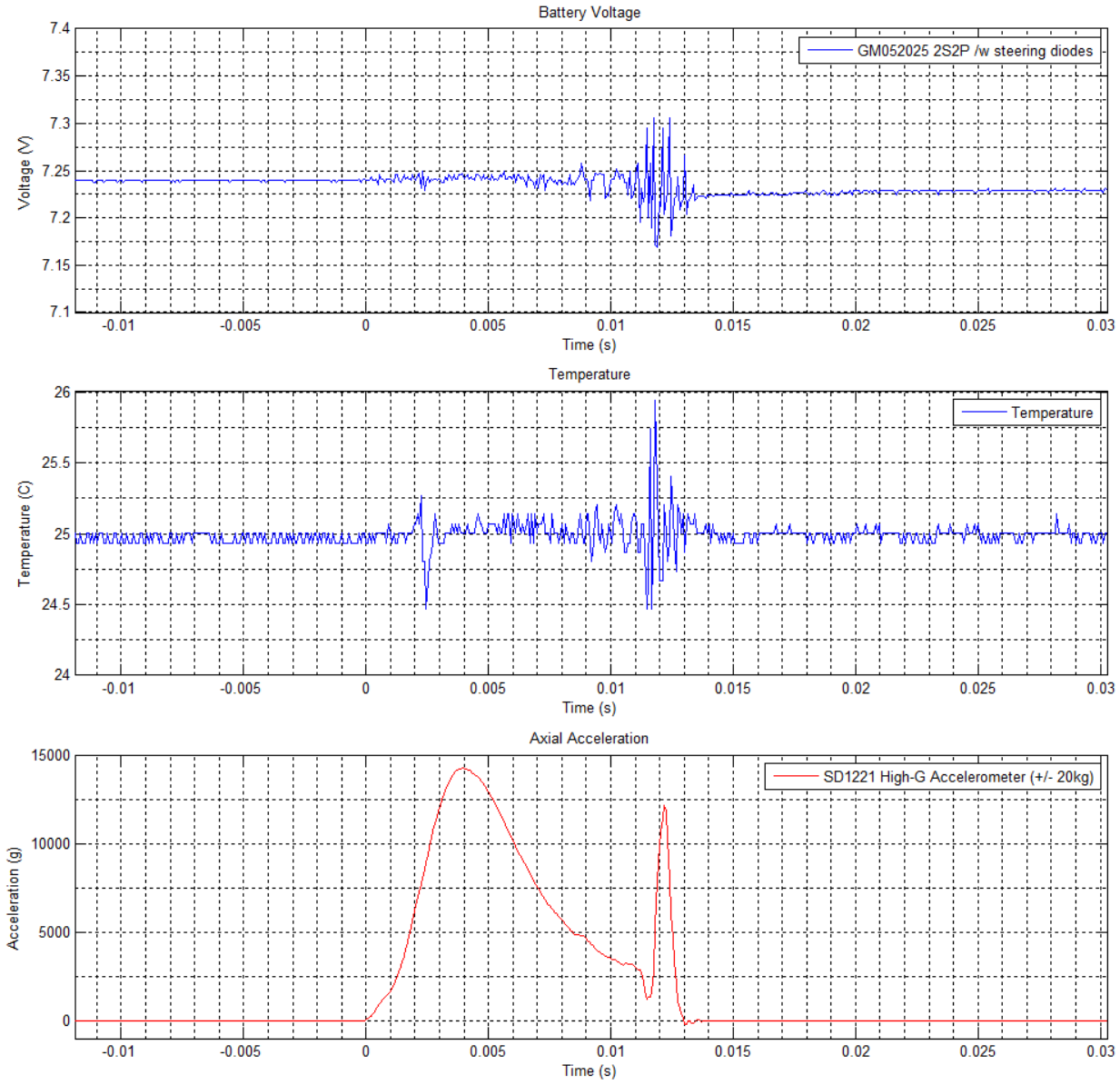

Figure 15
Plot of battery voltage and temperature measurement during the in-bore event

High-rate Gyroscopes (3X ADXRS649)

During gun launch, high-rate gyroscopes gave erroneous measurements, consistent with the results of prior air gun testing. The axial gyroscope was saturated during tube exit, which is expected given that the spin rate of the projectile exceeds sensor range. The other gyroscopes recovered and settled back to zero after tube exit. Figure 16 shows a plot of measurements from the three high-rate MEMS gyroscopes during the in-bore event. High-g axial accelerometer data is also plotted.

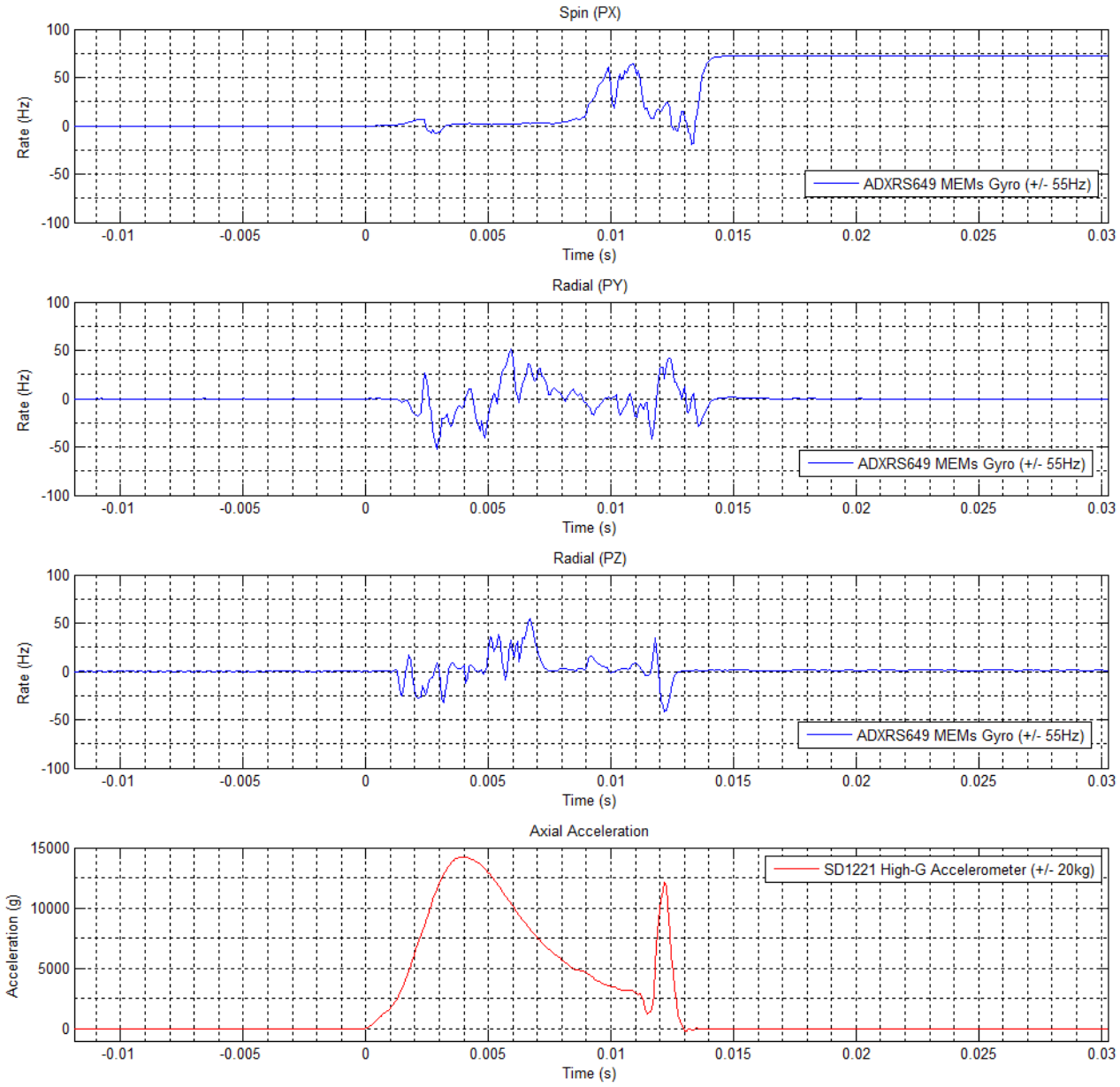

Figure 16
Plot of measurements from the three high-rate MEMS gyroscopes during in-bore event

Low-rate Gyroscopes (3X LY3100ALH)

The three low-rate gyroscopes gave erroneous data during gun launch. Saturation and oscillations were observed. Figure 17 shows measurements from the low-rate MEMS gyroscopes during the in-bore event.

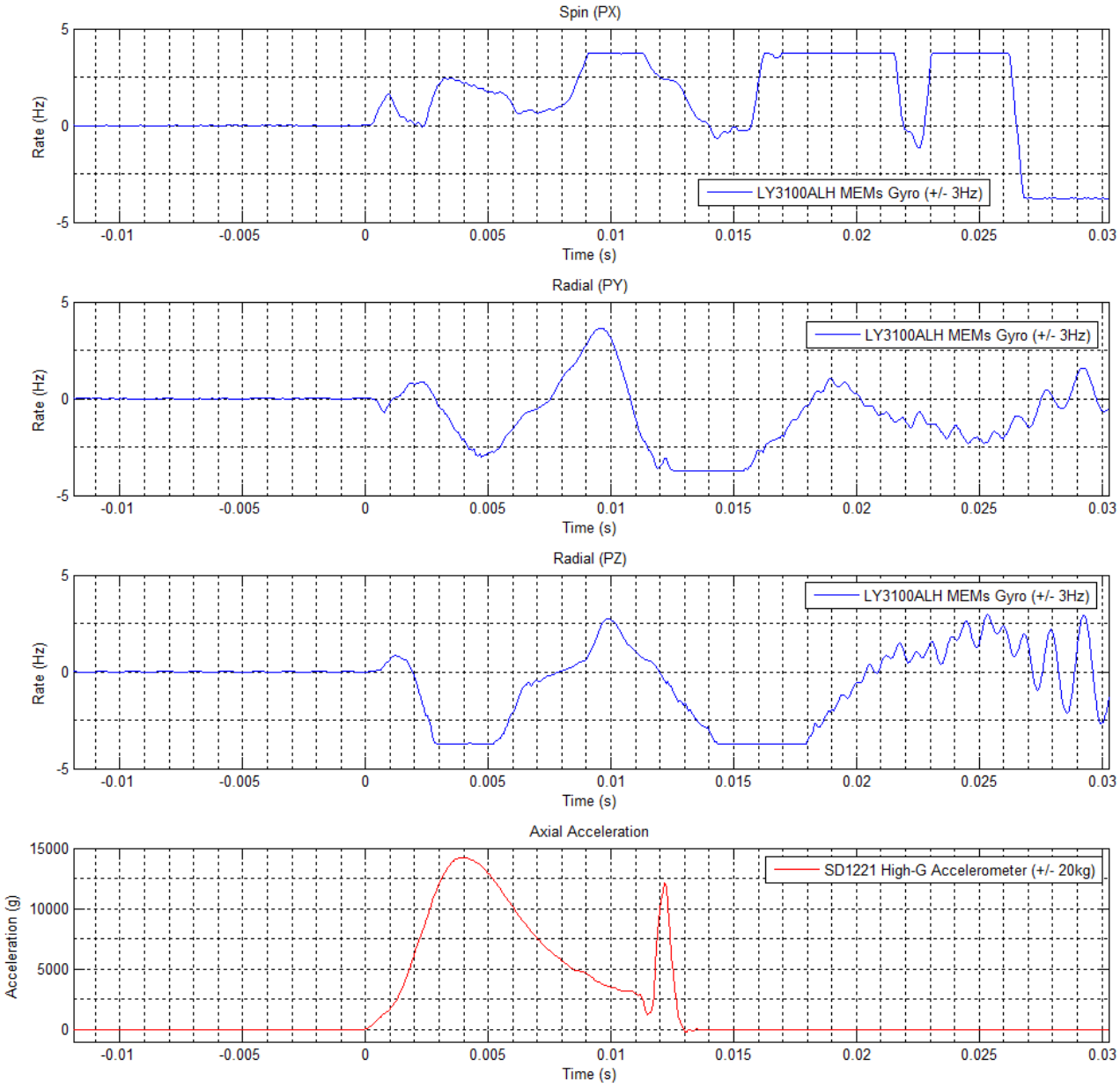

Figure 17
Measurements from low-rate MEMS gyroscopes during in-bore event

Ground Channel

A channel measuring circuit ground is included as part of the data stream. It is used as a diagnostic and should measure 0 volts at all times. Anything contrary indicates an issue with data acquisition on the Aerofuze. During setback, this channel was always measuring 0 volts. Figure 18 shows the measurements of the ground channel during the in-bore event.

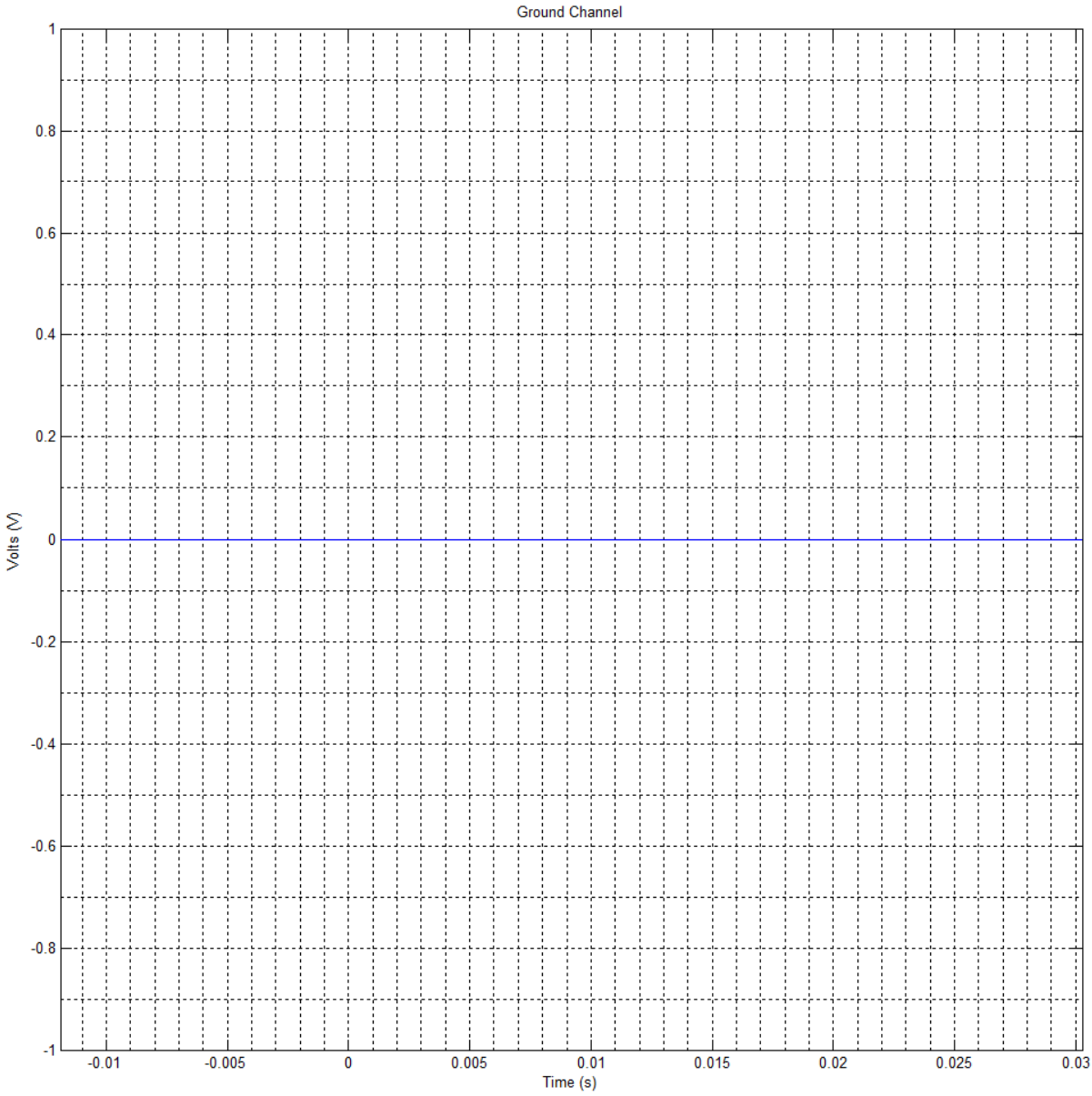

Figure 18
Measurements of the ground channel during in-bore event

In-flight Data

High-g Accelerometers (SD1221-20K)

High-g accelerometer data is clean and complete throughout the projectile flight with no evidence of sensor failure. Axial acceleration remains near 0 g throughout most of the flight. Radial acceleration in the py and pz directions were detected as 2,000 and 2,190 g, respectively, immediately after gun launch due to centrifugal force from spin and gradually reduced to 1,139 and 1,151 g, respectively, toward the end of flight. Figure 19 shows the measurements from the high-g accelerometers during flight.

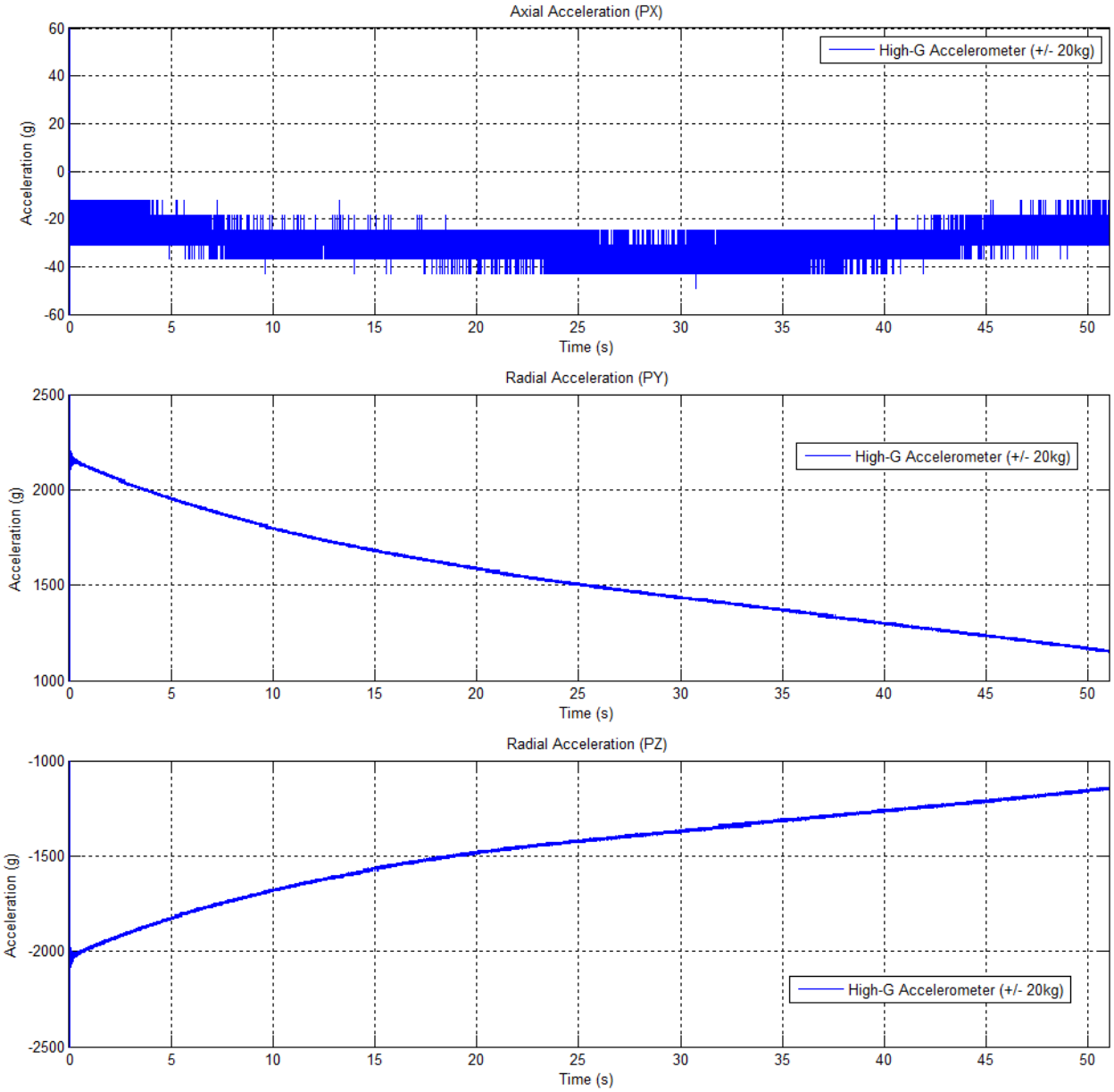

Figure 19
Measurements from the high-g accelerometers during flight

Low-g Accelerometer (ADXL377)

Low-G accelerometer data is available and was clean and complete throughout the projectile flight. Axial acceleration remains near 0 g throughout most of the flight, as corroborated with the high-g accelerometers. Drag can be observed, which gradually decays over the flight. Radial acceleration in the py and pz directions were detected as approximately 50 and 90 g, respectively, immediately after gun launch due to centrifugal force. These measurements gradually reduce to 27 and 36 g, respectively, toward the end of the flight. This sensor was positioned to be on-center with the axis of rotation; therefore, the measurement of centrifugal force was unexpected. Figure 20 shows the measurements from the low-g tri-axial accelerometer during flight.

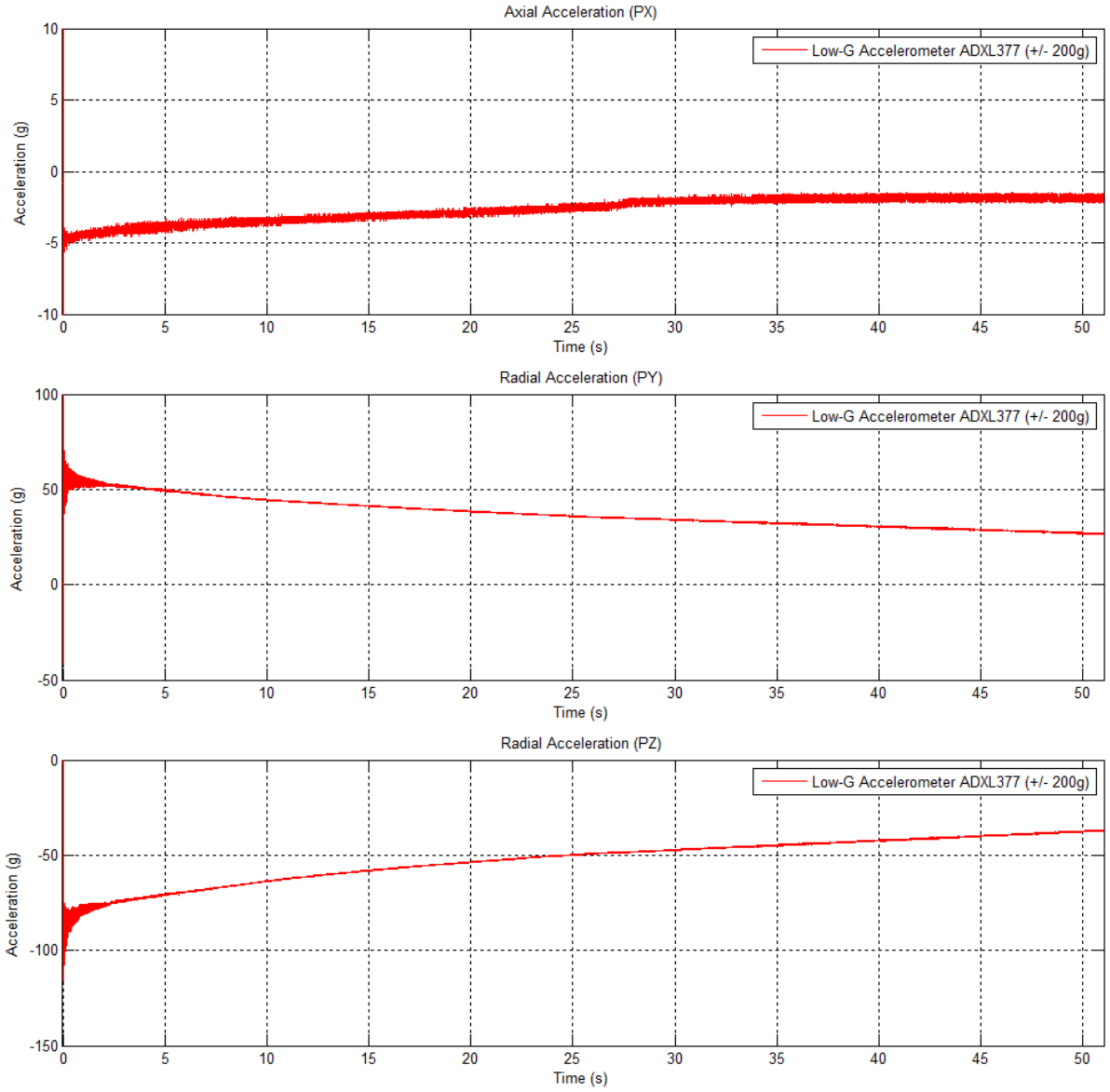

Figure 20
Measurements from the low-g tri-axial accelerometer during flight

It should be noted that, assuming 270 Hz of axial spin, 50 and 90 g of measured centrifugal acceleration corresponds to the 0.170 and 0.307-mm offset from the center axis, respectively. Prominent oscillations on the radial axes are noted within the first few seconds of flight, which gradually dampen up to 3 sec after gunfire. The oscillations measured have a fundamental frequency of 250 Hz with several overtones noted as well immediately after tube exit. These oscillations were not observed on the axial axis. Figure 21 shows the low-g accelerometer data within the first 0.3 sec of flight.

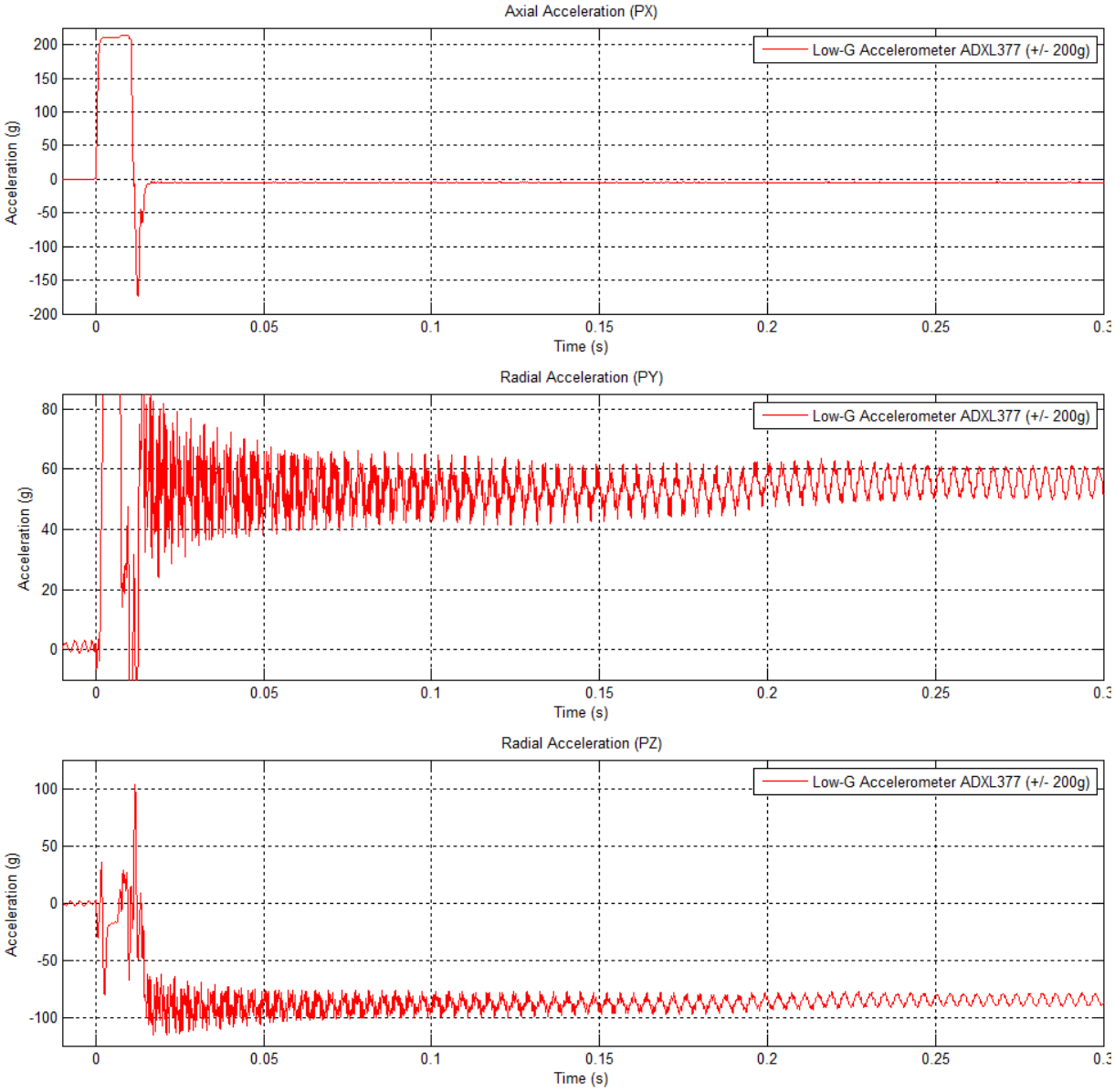

Figure 21
Low-g accelerometer data within the first 0.3 sec of flight

Magnetometer Data (2X HMC1053)

Magnetometer data is clean and complete throughout most of the flight for both sensors; however, some anomies were seen on Mag1 near 3.5 and 10 sec after time of fire. As expected, Mag1 pz data is unavailable, as this channel was noted to be not functional during assembly prior to the air gun testing. The Mag1 and Mag2 in the py axis track together very well and show a sinusoidal oscillation consistent with spin. The Mag1 and Mag2 data in the px axis is consistent with projectile flight. Figure 22 shows the magnetometer data during flight. Figure 23 shows the same data but is focused on 19.5 to 19.6 sec after time of fire.

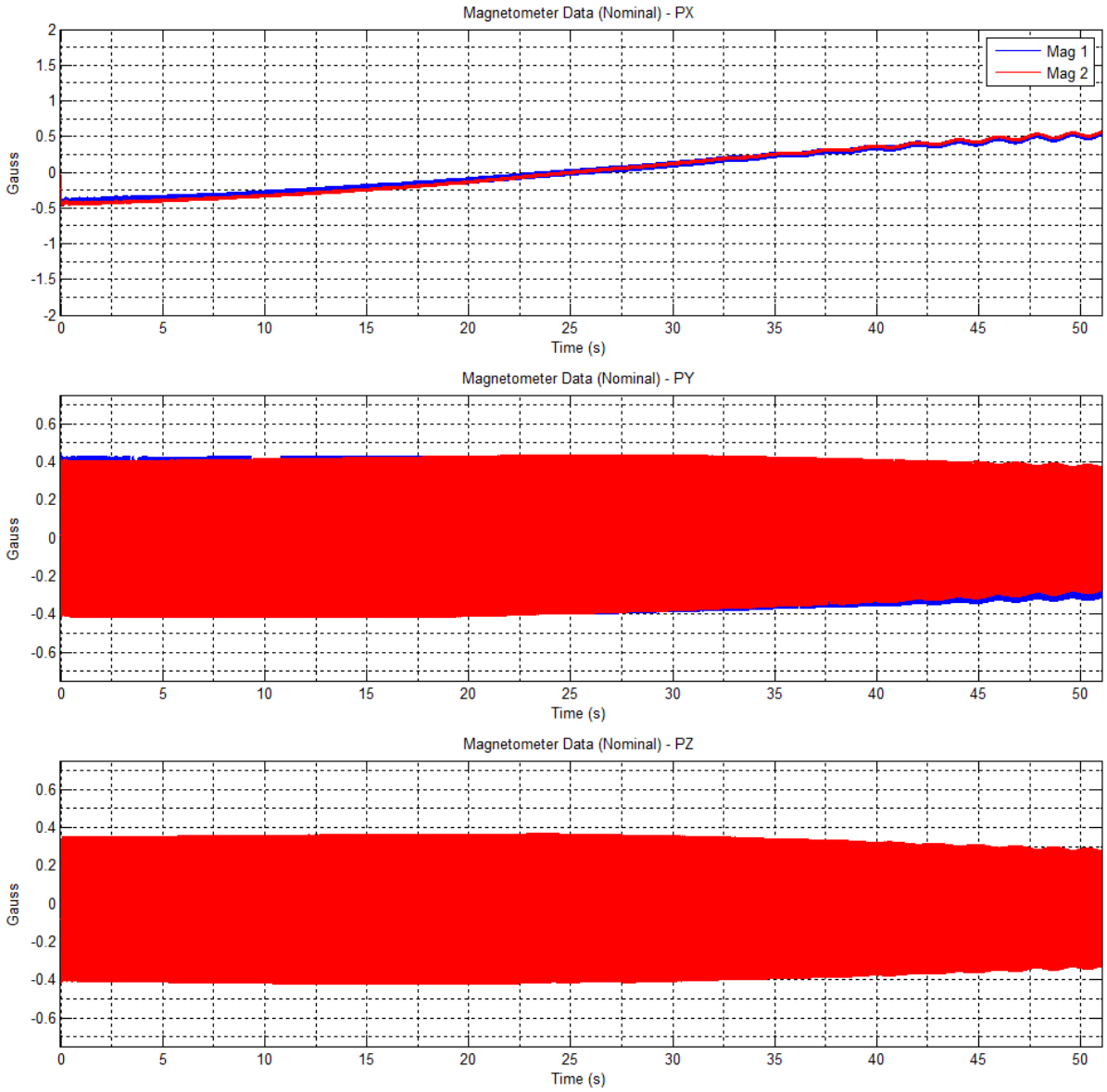

Figure 22
Magnetometer data during flight

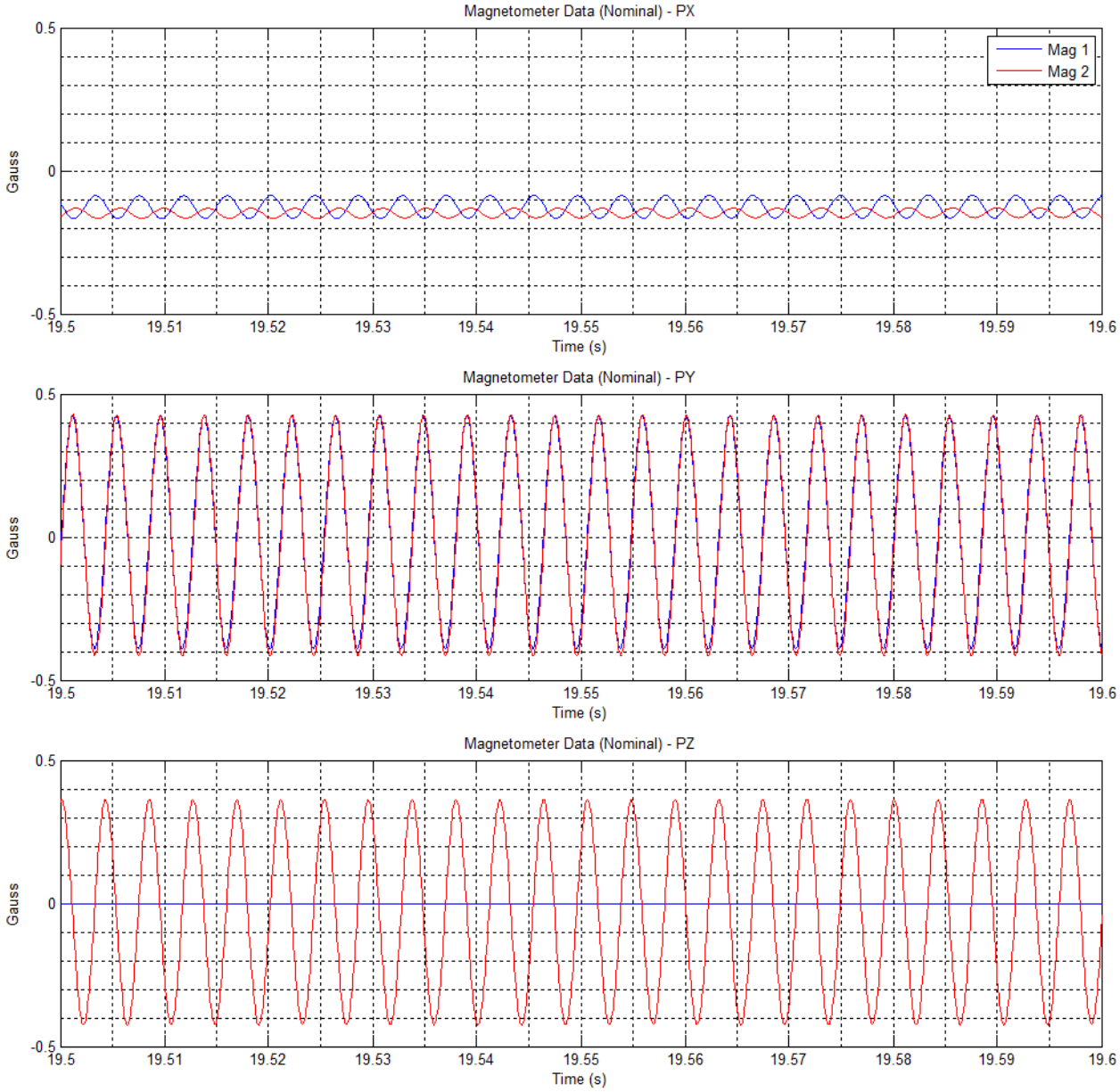

Figure 23
Magnetometer data during flight, focused on 19.5 to 19.6 sec after time of fire

A set of sliding short-time Fourier transform (STFT) spectrograms for the working magnetometer channels is given in figure 24. Overlaid on each plot is a curve that follows the peak of the spectrogram, which can be used as an estimate of projectile spin rate. The anomalies seen in the Mag1 py data is discussed later in this report. The Mag1 spectrum pz data is not available, as the channel was not functioning.

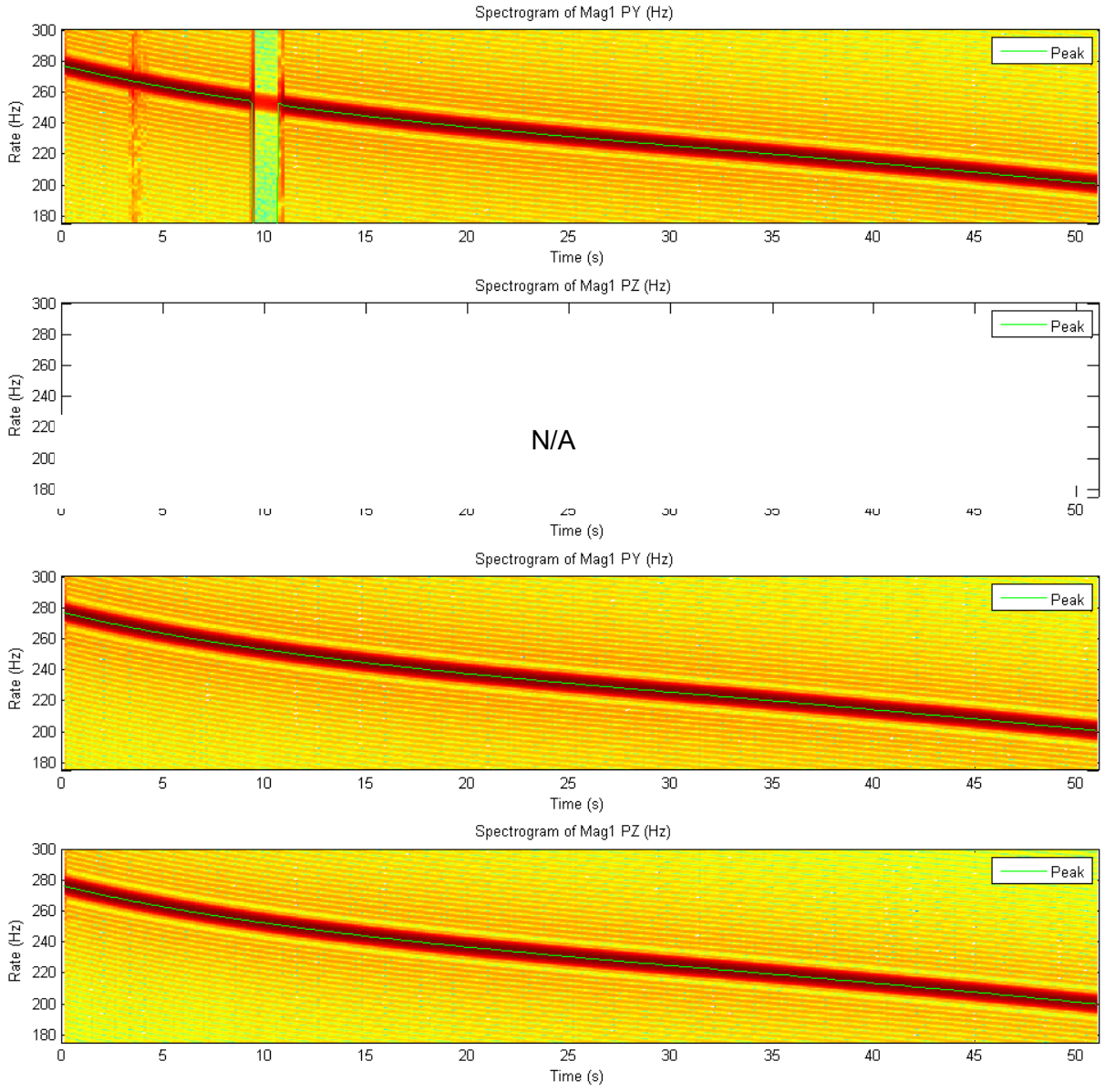

Figure 24
STFT spectrogram of magnetometer data during flight with peak frequency curve traced

Battery Voltage and Temperature

Battery voltage remained above 7.1V throughout the entire flight. Voltage gradually reduced from 7.22V at 20 ms after time of fire to 7.21V at 15 sec after time of fire. Oddly, the voltage gradually rises after this time period to 7.27V at 51 sec after time of fire. One explanation is that the voltage initially drops due to usage but then rises due to aeroballistics heating. Temperature was initially measured as 25°C (77°F) within the first few seconds of flight. While observing this, the temperature gradually rose to 42°C (107.6°F) toward the end of flight. This temperature rise was not expected; one explanation is that the unit was experiencing aeroballistics heating. Figure 25 shows plots of battery voltage and temperature during flight.

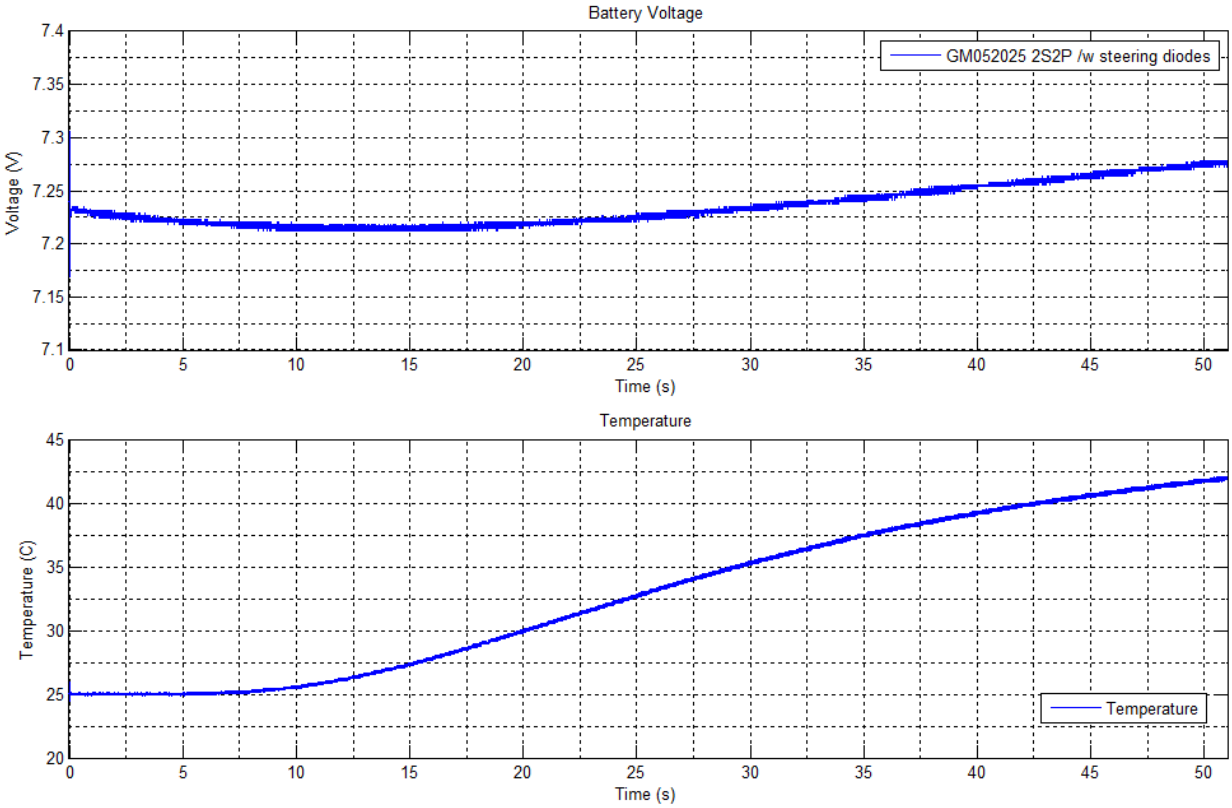

Figure 25
Plots of battery voltage and temperature during flight

High-rate Gyroscopes (3X ADXRS649)

Data from the high-rate gyroscopes were available during the entire flight with no evidence of sensor failure. As expected, the axial high-rate gyroscope was pegged at +72 Hz, well beyond its rated measurement range of +55 Hz, due to the round spinning at approximately 270 Hz. The radial high-rate gyroscopes (measuring pitch and yaw) remained near 0 Hz throughout the entire flight; however, some offset can be seen. Figure 26 shows a plot of measurements from the three high-rate MEMS gyroscopes during flight.

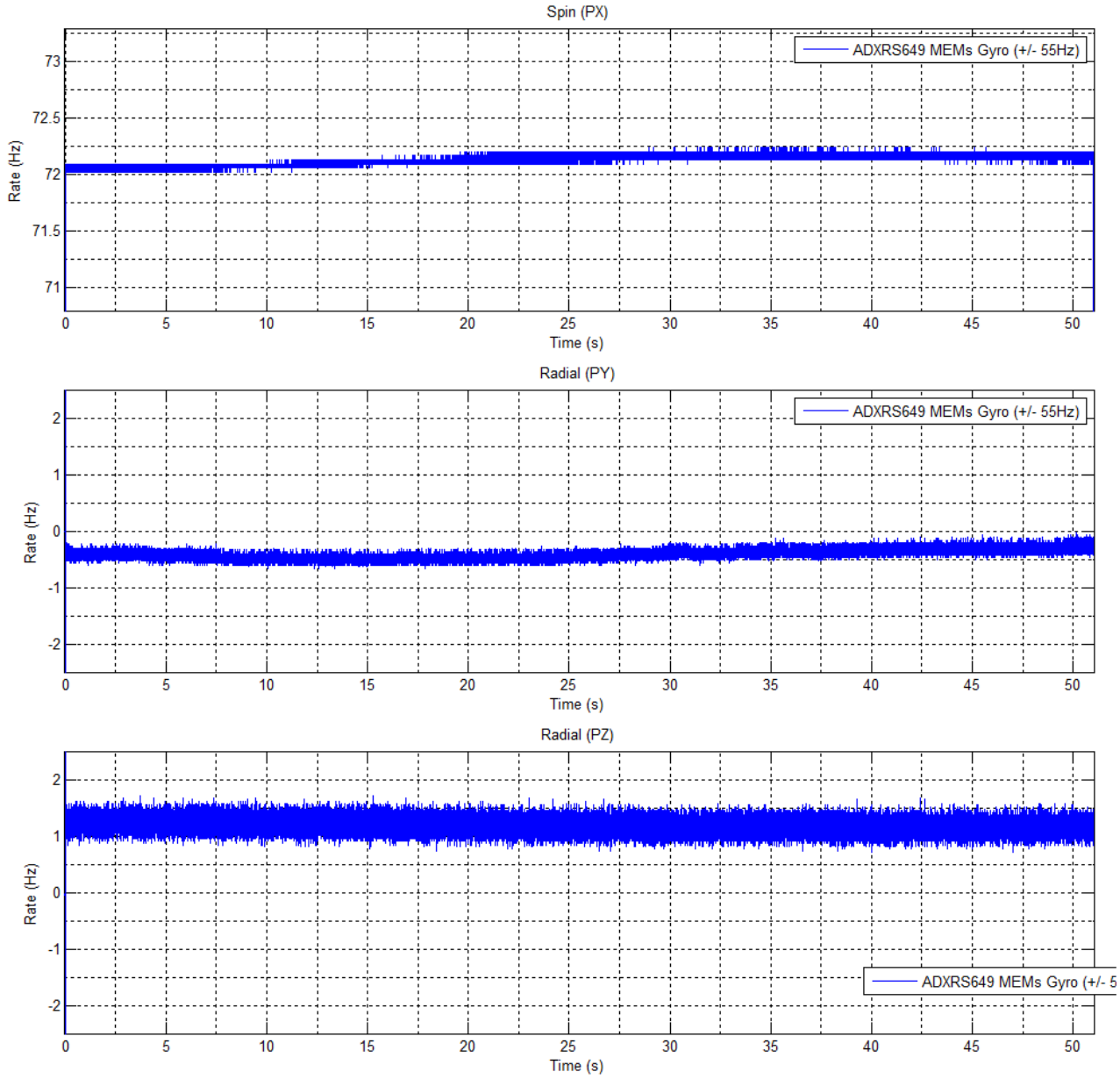

Figure 26
Plot of measurements from the three high-rate MEMS gyroscopes during flight

Low-rate Gyroscopes (3X LY3100ALH)

Data from the three low-rate gyroscopes were available during the entire flight; however, all of the sensors were pegged at beyond their measurement range. The axial low-rate gyroscope is railed at 3.7 Hz, as expected, due to the high-spin rate of the round. The other gyroscopes are railed above their specified limits but do show a gradual decline toward the end of flight. It was unexpected that the radial low-rate gyroscopes would saturate. One explanation is that the cross-axis sensitivities of the gyroscopes are enough to saturate them under a high-spin rate. A small glitch is observed with the yaw gyroscope at 1.08 sec after time of fire. Figure 27 shows a plot of measurements from the three low-rate MEMS gyroscopes during flight.

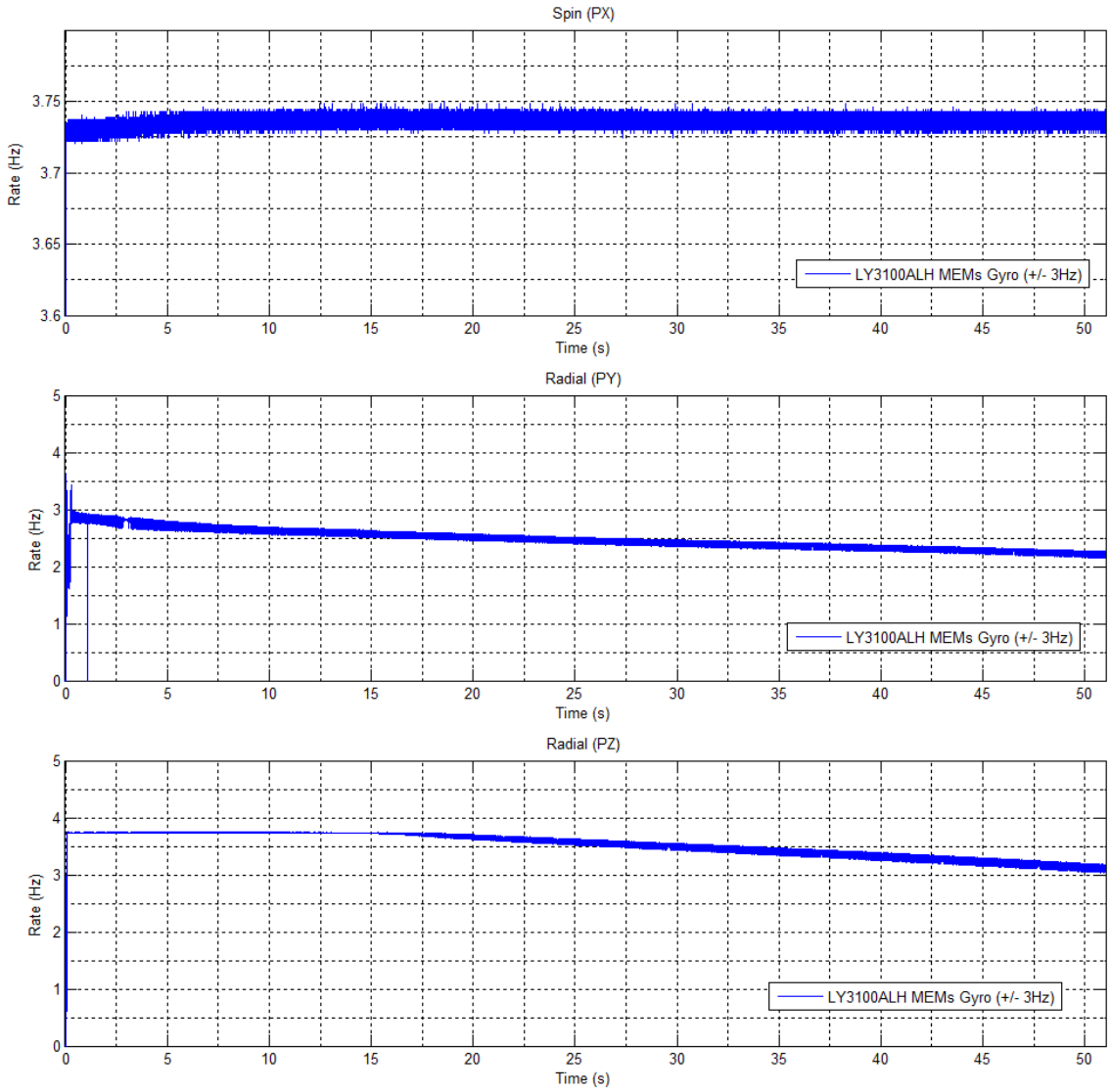

Figure 27
Plot of measurements from the three low-rate MEMS gyroscopes during flight

Runtime Counter

A runtime counter was included as a diagnostic that counts whole seconds from the time the system is turned on. Recorded data starts at 174 sec (2:54) with setback at 189 sec (3:09) and end of data at 240 sec (4:00). This counter did not reset to zero, which indicates no system resets occurred. Figure 28 shows a plot of the runtime counter channel during flight.

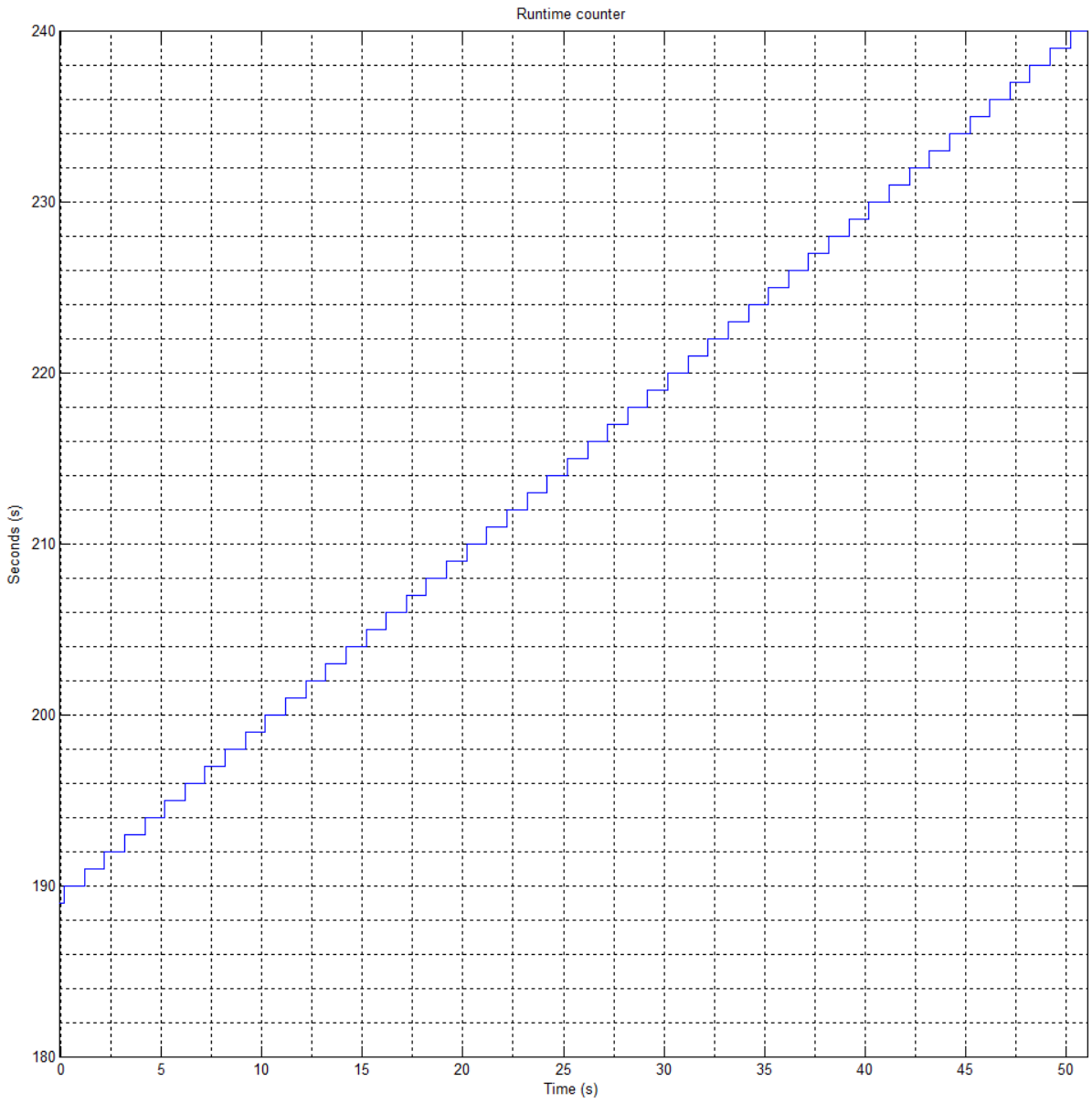

Figure 28
Plot of runtime counter channel during flight

Ground Channel

A channel measuring circuit ground is included as part of the data stream. It is used as a diagnostic and should measure 0 volts at all times. Anything contrary indicates an issue with data acquisition on the Aerofuze. During flight, this channel was always 0 volts. Figure 29 shows a plot of the ground channel during flight.

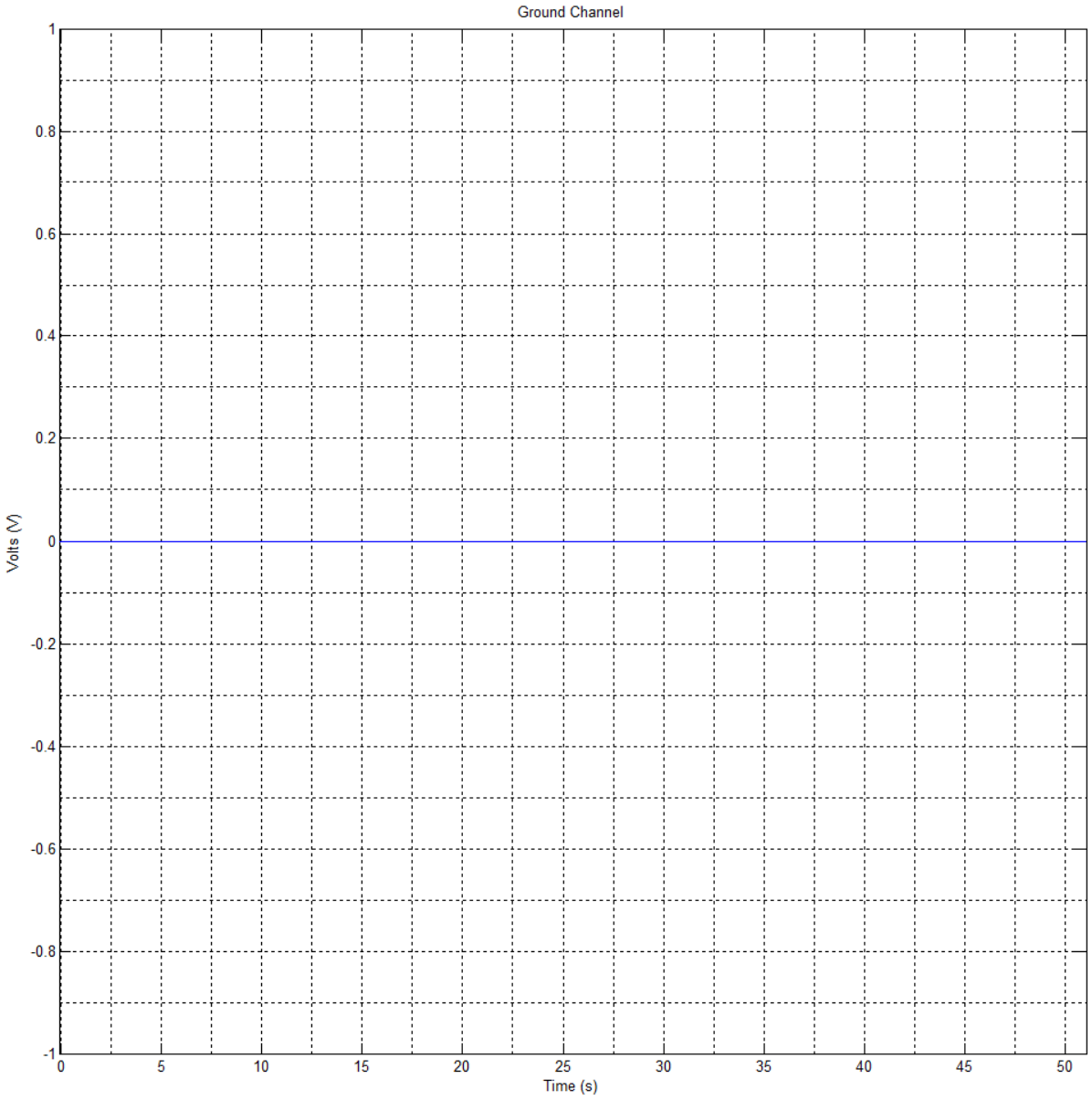

Figure 29
Plot of ground channel during flight

Derived Quantities

Integrated Velocity and Distance Travelled

Integrating the acceleration curve during the in-bore event yields a muzzle exit velocity of 876.1 m/s and a travel distance of 6.11 m. The exit velocity can be compared to the Doppler radar measured muzzle exit velocity of 843.3 m/s for the projectile. Figure 30 shows estimates of projectile velocity and distance travelled that was derived from an integration of the high-g acceleration curve, which is also shown.

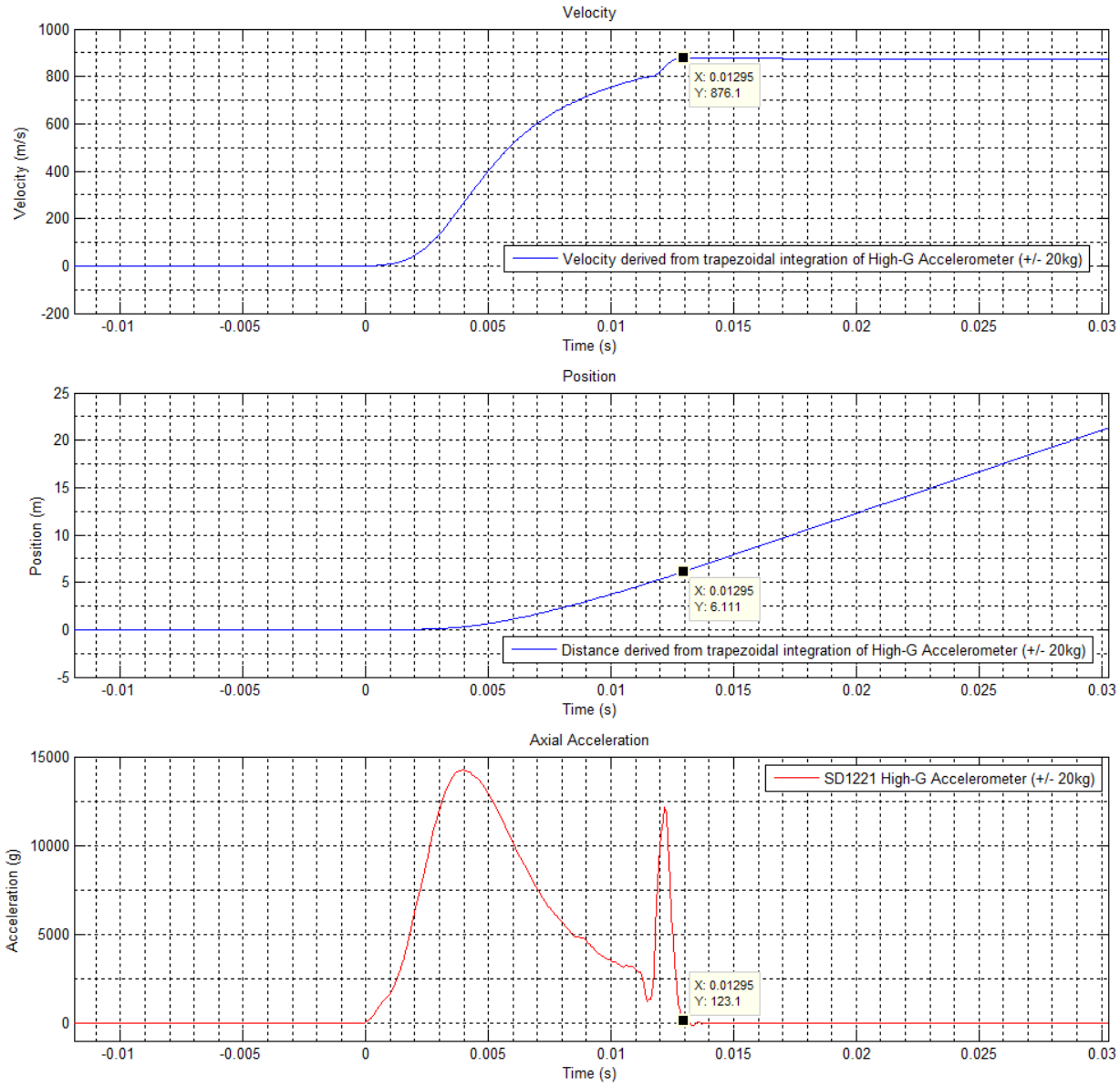

Figure 30
Estimates of projectile velocity and distance travelled, derived from an integration of the high-g acceleration curve (also shown)

Axial Spin Rate

Axial spin rate was derived in post-processing from the centrifugal force measured from the two radial high-g accelerometers. The spin rates are computed assuming that each accelerometer sensing element is 0.282 in. offset from center using the formula ($a = r\omega^2$). The rates are plotted in figure 31, along with the peak of the Mag2 pz spectrogram plot. This yields a spin rate that starts at 265 to 276 Hz depending on the sensor used and gradually declines to 199 Hz toward the end of flight. Spin rate as measured from the high-rate axial gyroscope is also shown but is pegged at 72 Hz. Saturated spin rate from the low-rate axial gyroscope is also plotted.

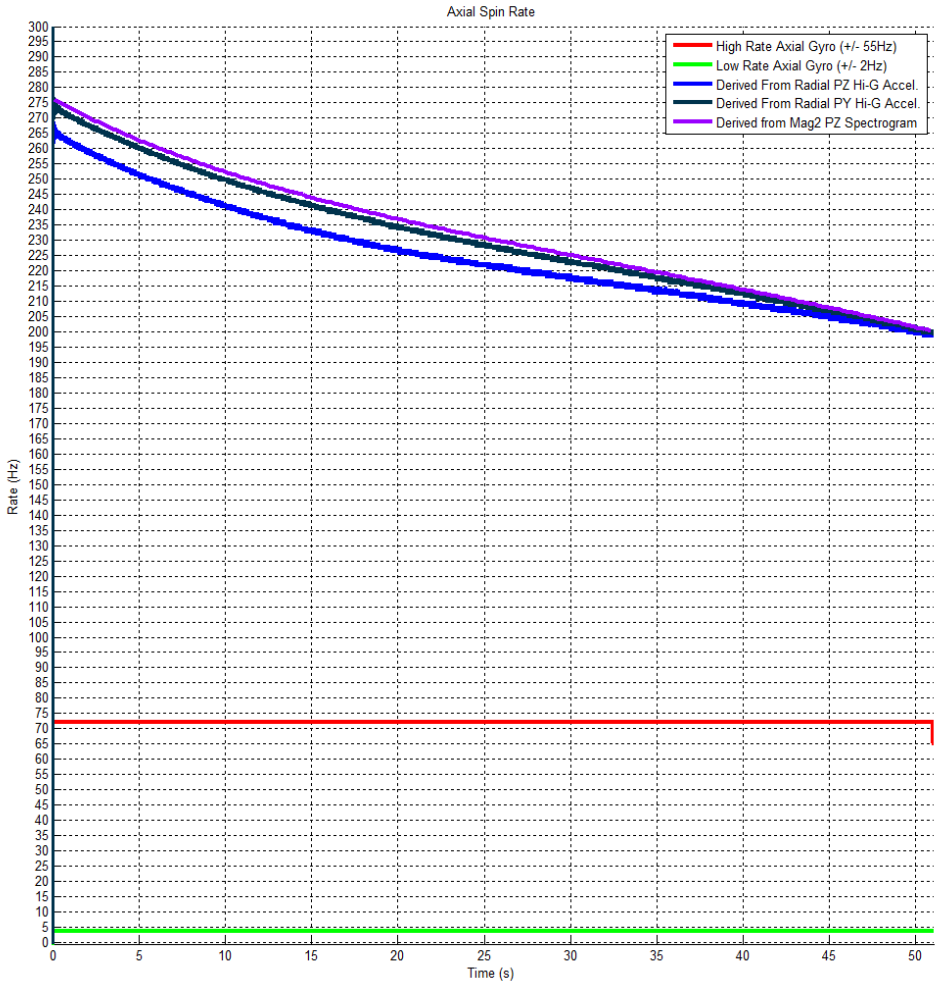

Figure 31
Plot of axial spin rates derived from radial high-g accelerometers, nominal Mag2 pz spectrogram peak frequencies, and gyroscopes

The spin rate can also be estimated from the muzzle exit velocity measured by the Doppler radar (843.3 m/s) and the twist rate of the M777 gun tube rifling (1/20 rev/caliber). This yields 1 revolution per 3.1 m/s of velocity and, hence, a muzzle exit spin rate of 272.03 Hz, which is in good agreement with the spin rates estimated from the functioning on-board sensors.

Unexpected Data

- The system temperature rose significantly during flight.
- Low-rate gyroscopes on the pitch and roll axes are in saturation.
- Low-g radial acceleration channels measured centrifugal force from spin.

Anomalous Data

- A small ringing was observed on the measured temperature channel during setback.
- The centrifugal force measured from the two radial accelerometers are different, despite that both accelerometers are designed to have the same offset from the projectile center axis. There is a slight deviation between the two that converges toward the end of flight, as plotted in figure 32.

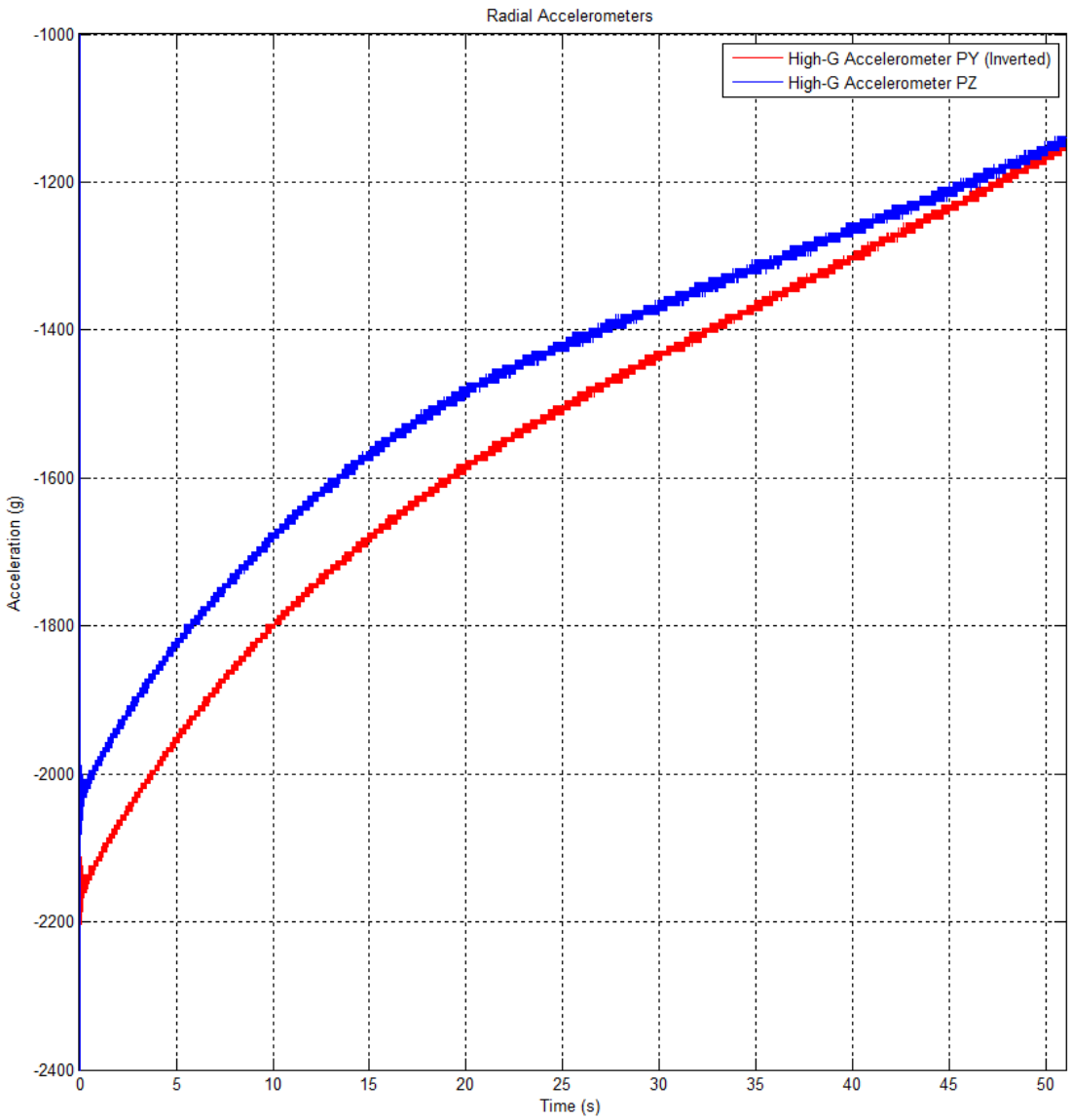

Figure 32
Comparison of high-g radial accelerometer measurements

Measured data from Mag1 in the calibrated y-axis shows amplitude and phase changes for two brief periods of time (3 to 4 sec after time of fire, 9 to 11 sec after time of fire). A small change in amplitude is also seen in Mag1 on the calibrated z-axis. The channels recover after these time periods. Interestingly, the frequency of oscillation is maintained during these time periods, and only amplitude and phase are affected. These anomalies were not observed in Mag2. Figure 33 shows plots of Mag1 channels showing anomalies (middle) between 3 and 11 sec into flight. Figure 34 shows plots of anomalies on Mag1 py channels at 3.4 to 3.7 sec (top), 9.2 to 9.5 sec (middle), and 10.5 to 10.8 sec (bottom).

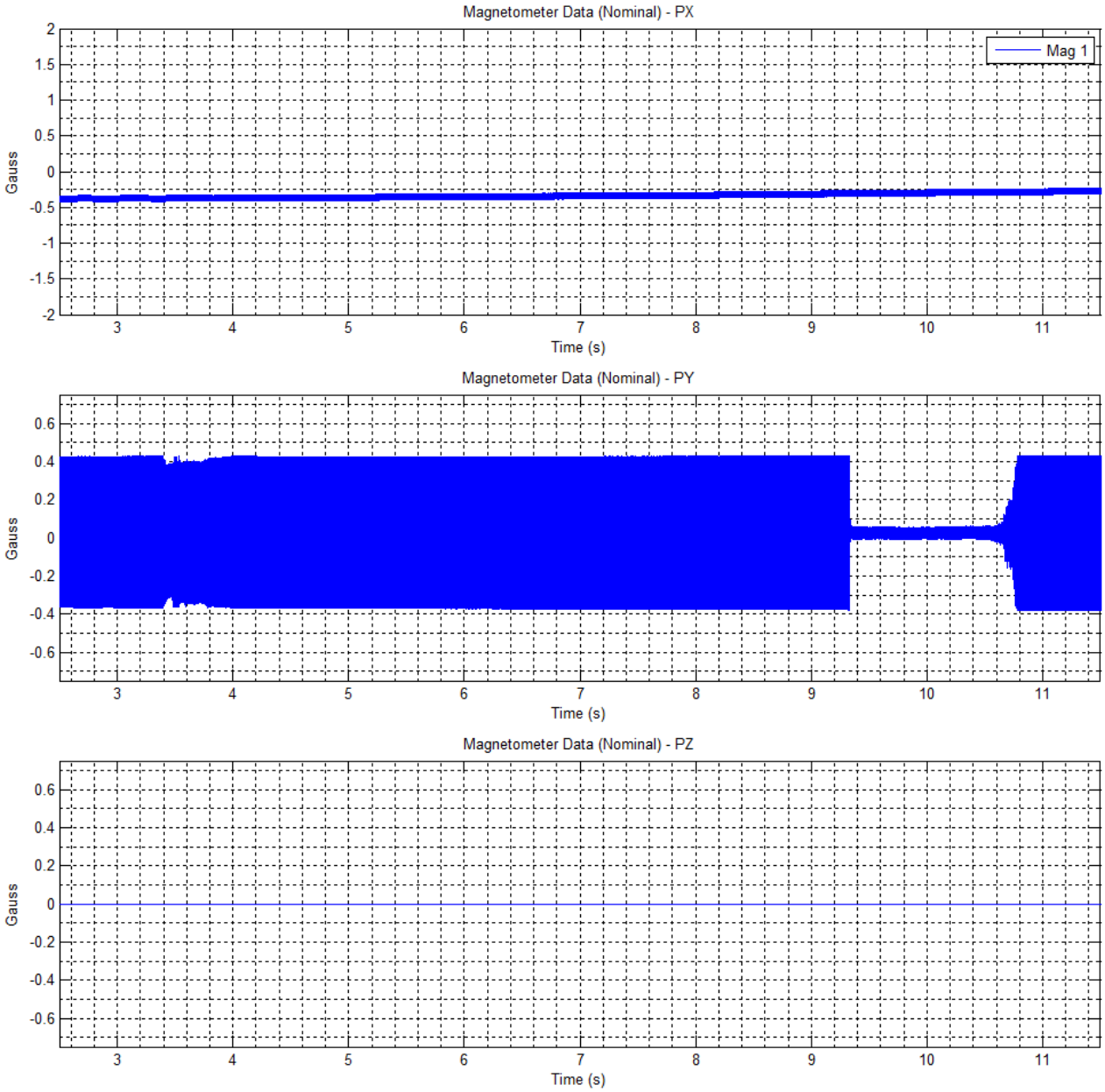

Figure 33
Plots of Mag1 channels showing anomalies (middle) between 3 and 11 sec into flight

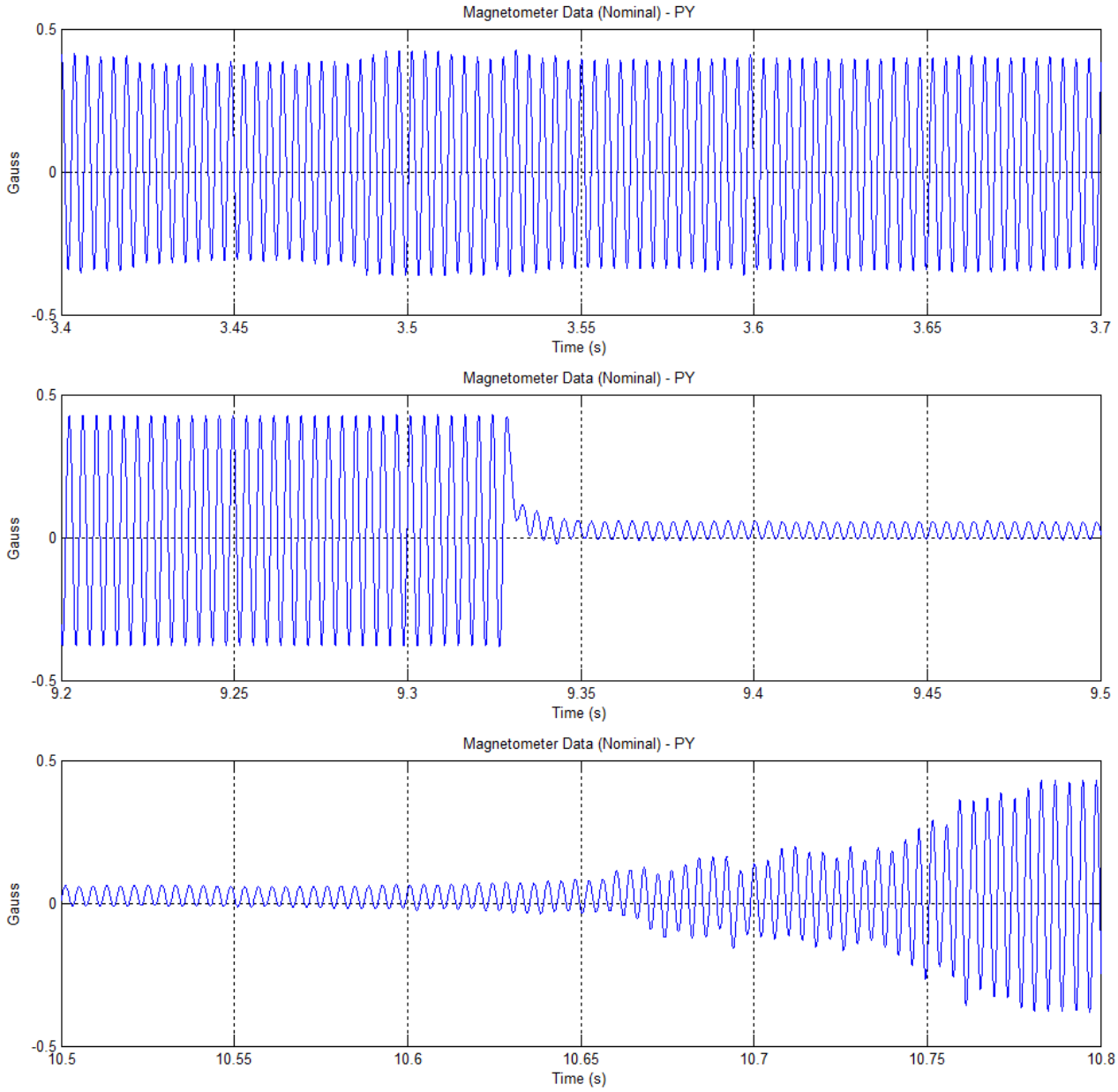

Figure 34
Plots of anomalies on Mag1 py channels at 3.4 to 3.7 sec (top), 9.2 to 9.5 sec (middle), and 10.5 to 10.8 sec (bottom)

CONCLUSIONS

The Aerofuze system was capable of capturing the required in-flight data of an M795 projectile spinning at nearly 300 Hz. The data was captured with a high enough fidelity to be used in an exterior ballistics analysis and with enough redundancies to overcome the magnetometer channel failures and anomalies that occurred. Spin rate measured from the magnetometers provide an excellent measurement of the spin rate of the projectile and are in good agreement with estimates from the other sensors and radar data. The micro-electromechanical systems (MEMS) accelerometers on the system captured an abundance of data, including setback, set forward, drag, and centripetal force due to spin with no evidence of sensor failure. The MEMS gyroscopes saturated due to the high spin rate; however, they show no evidence of failure. Though not by design, the in-bore data was captured completely. However, it was not captured with a high enough sampling rate to be used in an interior ballistics analysis. Future designs of the Aerofuze system might have this feature. The in-bore data can be used to observe the gun-launch responses of the sensors that were used. The Aerofuze system succeeds in its goal of acting as a diagnostic telemeter for fast-spinning artillery projectiles.

REFERENCES

1. Harkin, T. and Don, M., “Achieving High Resolution Measurements Within Limited Bandwidth Via Sensor Data Compression,” ARL-RP-444, U.S. Army Research Laboratory, Aberdeen Proving Ground, MD, 2013.

BIBLIOGRAPHY

1. Barton, A., “Memorandum for Record: Report on Aerofuze Test at the KOFA Range, Yuma Proving Grounds, AZ, 19 May 2015,” Memorandum, U.S. Army ARDEC, Picatinny Arsenal, NJ, 19 May 2015.

2. Bukowski, E.F., “Evaluation of Commercial-off-the-Shelf Lithium Batteries for Use in Ballistic Telemetry Systems,” Technical Report ARL-TR-4840, U.S. Army Research Laboratory, Aberdeen Proving Ground, MD, June 2009.

3. Karlsen, A.J., “Ballistic Simulator Shock Testing of Armament Components,” Technical Report ARAED-TR-86040, U.S. Army ARDEC, Picatinny Arsenal, NJ, December 1986.

4. Cordes, J.A., Lee, J., Hader, G., Reinhardt, L., Kessler, C., Gray, N., and Guevara, M.A., “Statistical Comparisons Between Qualification Tests for Gun-Fired Projectiles,” ASME Journal of Applied Mechanics, vol. 77, no. 5, 2010.

5. Burke, L.W., Bukowski, E., Newnham, C., Scholey, N., Hoge, W., and Ye, Z., “HSTSS Battery Development for Missile and Ballistic Telemetry Applications,” Technical Report ARL-MR-477, U.S. Army Research Laboratory, Aberdeen Proving Ground, MD, May 2000.

DISTRIBUTION LIST

U.S. Army ARDEC
ATTN: RDAR-EIK
RDAR-MEF, E. Persau
F. Loso
D. Troast
RDAR-MEA-A, M. Hollis
E. Marshall
G. Dundon
M. Hawkswell
J. Cordes
RDAR-MEF-I, C. Sandberg
P. Sweeney
R. Granitzki
J. Choi
D. Hoch
A. Barton
RDAR-MEF-P, R. Marchak
RDAR-MEF-A, T. Recchia
W. Koenig
W. Toledo
R. Trohanowsky
RDAR-EIQ-PE, J. Heiskanen
RDAR-EIQ-EC, M. Menegus
Picatinny Arsenal, NJ 07806-5000

Defense Technical Information Center (DTIC)
ATTN: Accessions Division
8725 John J. Kingman Road, Ste 0944
Fort Belvoir, VA 22060-6218

GIDEP Operations Center
P.O. Box 8000
Corona, CA 91718-8000
gidep@gidep.org

U.S. Army ARL
ATTN: RDRL-WML-F, B. Davis
T. Harkins
M. Don
R. Hall
Aberdeen Proving Ground, MD 21005-5069

REVIEW AND APPROVAL OF ARDEC TECHNICAL REPORTS

Report on the 155MM M795 Aerofuze Test at the KOFA Range, Yuma Proving Grounds, AZ, 19 May 2015
Title

Date received by LCSD

Aaron Barton
Author/Project Engineer

Report number (to be assigned by LCSD)

x3521 | 95
Extension | Building

Precision Munitions Instrumentation Division
Author's/Project Engineers Office (Division, Laboratory, Symbol)

PART 1. **Must be signed before the report can be edited.**

a. The draft copy of this report has been reviewed for technical accuracy and is approved for editing.

b. Use Distribution Statement A ✓, B____, C____, D____, E____, F____ or X____ for the reason checked on the continuation of this form. Reason: _____

1. If Statement A is selected, the report will be released to the National Technical Information Service (NTIS) for sale to the general public. Only unclassified reports whose distribution is not limited or controlled in any way are released to NTIS.

2. If Statement B, C, D, E, F, or X is selected, the report will be released to the Defense Technical Information Center (DTIC) which will limit distribution according to the conditions indicated in the statement.

c. The distribution list for this report has been reviewed for accuracy and completeness.

Craig Sandberg
26 MAY 2016
(A) Division Chief (Date)

PART 2. To be signed either when draft report is submitted or after review of reproduction copy.

This report is approved for publication.

Craig Sandberg
29SEP 2017
Division Chief (Date)

Andrew Pskowski
6/11/16
RDAR-CIS (Date)

LCSD 49 supersedes SMCAR Form 49, 20 Dec 06